Effects of gradual increase of kaolinite concentration on experimental turbidity current flow dynamics and related deposits

Johana Melissa Ramirez Bernal
Supervisor: Dr. J. T. Eggenhuisen
Second supervisor: Dr. M.B Cartigny

MSc-thesis • Faculty of Geosciences • Utrecht University •**15/04/2013**

Universiteit Utrecht

Table of Contents

Abstract

Clay particles are common elements in many natural flows such us fluvial, lacustrine and deep water flows. The addition of a small amount of clay causes changes in the fluid-dynamics of a flow and in the architecture of depositional systems. The understanding of these effect are important to correlate and characterize better outcrops deposits and buried reservoirs of oil and gas. Eleven successful laboratory experiments with a constant 13% volume concentration were performed. Five runs correspond to the first set of experiments that have different ratios between sand and clay at a constant slope angle of 9 degrees at which all sand was bypassing. Six more runs correspond to two additional sets of experiments with constant sediment fraction but decreasing slope angles (clay at 4% sand at 9% vc in the first set and 13% sand 0% clay vc in the second set). There is a decreasing trend in Umax, and shear velocities as the clay content becomes higher, also the distance between Umax and the bedding plane becomes higher with larger clay concentrations. Thickness and sedimentation rates increase as the slope and clay content decrease. Also sand body deposits show to be coarser-grained than the tail deposits and these being coarser-grained than the input sediment. Closed-channel fluid dynamics reveal to be comparable to open-channel flow-dynamics, since similar phases were observed as clay content increases (1) turbulent flow; (2) turbulence-enhanced transitional flow; (3) upper transitional plug flow; and (4) quasi-laminar plug flow, these transitions are explaining by the capacity of clay to suppress local shear stresses, reducing velocity gradient and turbulence intensity. Clay is more efficient than silt on reducing the equilibrium and thus enhance the transport efficiency of sand. When looking at the experiments as a window along the continental slope to the basin plane in real-world systems, thick coarse grained sandy-packages are generated at relatively low slopes in the laboratory, or distal parts in nature under a clay laden flow. On the other hand, free-clay laden flows produce thick coarse grained sandstones at higher angle slopes in the laboratory or proximal areas in nature. Finally is also demonstrated that clean sand packages can be deposited from clay-laden flows.

Introduction

The fluid-dynamic characteristics of a flow can be transformed by increasing the concentration of fine silts and clay. Flows with small concentrations of clay minerals retain its Newtonian properties, but once the concentration reaches a threshold value the clay particles start to develop strong interactions with each other creating electrostatic bonds that suppress turbulence and change the flow to a Non-Newtonian type (Wang and Larsen, 1994).

Because clay minerals are common elements in many natural flows, for instance high-density turbidity currents in lakes and seas (Lowe & Guy 2000, Haughton et al. 2009) subaerial mudflows in rivers (Wan & Wang, 1994) and lahars in volcanic environments (Best, 1992) the transition from Newtonian to Non-Newtonian flows is a common process that affects not only the geological record but also human populations living close by the flow influence area.

Turbidity flows are in principle Newtonian flows (Mulder & Alexander, 2001) that are forced by gravity and can transform its fluid-properties as the current erodes and incorporate sufficient clay that suppress turbulence (Haughton. 2009). A better understanding of the clay concentration required to cause turbulence damping, together with velocity structures and depositional character are necessary to better understand the fluid-dynamics of clay-laden flows and their associated deposits.

Since many large oil and gas fields have recently been encountered in turbidite deposits all over the world including areas in Nigeria, Gulf of Mexico, East cost of Australia, Brazil, etc (Albertão et al. 2011, McHargue et al. 2011), hydrocarbon exploration is increasingly moving into deep-water setting to meet the growing world demand for oil and gas. In order to minimise the risks during the exploration phase and obtain better development models it is vital to understand the subsurface distribution of turbidite deposits and therefore the processes affecting the turbidity flows that deposited these.

CLAY EFFECTS ON EXPERIMENTAL TURBIDITY CURRENTS

There is not any experimental work on the effects of clay on turbidity current flow structure. However, some investigations have shown that the addition of a small portion of fine grained materials enhances the carrying capacity and efficiency of density turbidity currents (Hofstra, 2011 & Gladstone, 1998). After Hofstra (2011) who studied the effects of silt in turbidity currents, the hypothesis is that the addition of small amount of clay will increase the transport efficiency even further.

Furthermore, Baas et al. (2002, 2008, 2009 & 2011) performed a series of experimental test in open channel flows varying the kaolin concentration. The authors described a more complex variation in velocity and turbulence structure than the notion of gradual turbulence damping in which five flow types can be distinguished as the clay content increases: 1.Turbulent flow (normally turbulent) 2. Turbulence-enhanced transitional flow (strongly turbulent) 3. Lower transitional plug flow (strong turbulence at the bottom and lower turbulence at the top) 4. Upper transitional plug flow (damped turbulence caused by gelling of the clay) 5. Quasi-laminar plug flow (turbulence is suppressed/gelling dominates) (Figure 1).

Particle support in muddy flows is controlled by the interplay of turbulence caused by shear stresses and cohesive forces (Sumner et al. 2009 and Baas et al. 2009). For instance, in a turbulent flow the amount of clay particles is not enough to develop strong cohesive forces and affect the flow structure. In Turbulence-Enhanced Transitional flows (TETF) the extra added amount of clay causes the development of a internal shear layer close to the base of the flow that causes a turbulence enhancement over the entire flow depth. Cohesive forces start to act in Lower Transitional Plug Flow (LTPF), and the electrostatic bonds between clay particles create a plug-flow region free of turbulence close to the water surface. As the clay amount increases in Upper Transitional Plug Flow (UTPF) the cohesive forces become stronger causing the plug area to move downwards and reduce the turbulence intensity below the internal shear layer. Finally in the Quasi-Laminar Plug Flow (QLPF) a rigid plug without internal deformation dominates and the turbulence forces are totally overpassed.

Following Baas et al. (2002, 2008 & 2009) and Sumner et al. (2009), a second hypothesis rises and is that the gradual increment of clay in closed systems (turbidity-flows) will also develop different types of flows distinguishable of each other by their own fluid-dynamics characteristics.

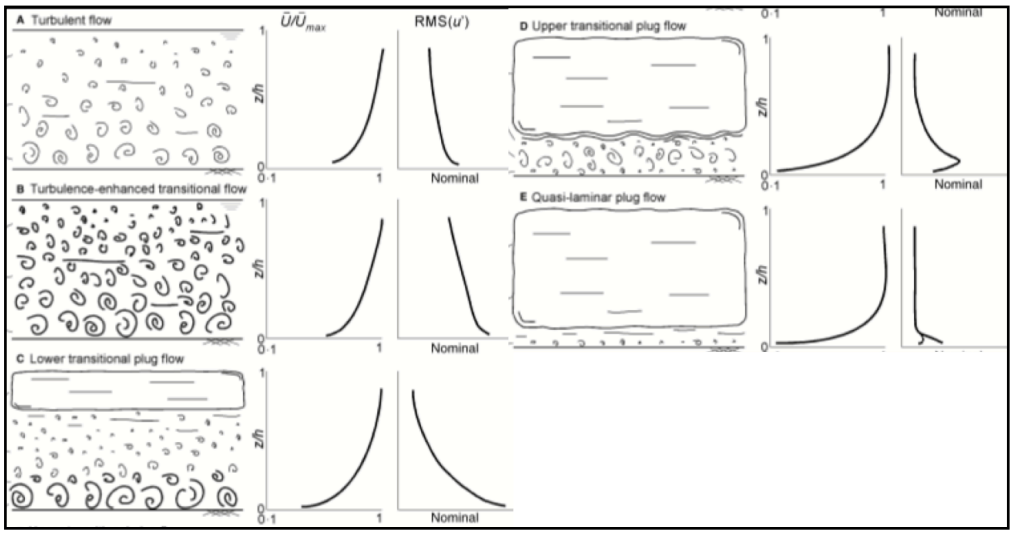

Fig. 1. Schematic models for the five different clay flow types defined in Baas et al. 2009. The graphs to the right of the models represent characteristic vertical profiles of dimensionless downstream velocity (U/Umax), root-mean-square of downstream velocity (RMS(u) and dimensionless turbulence intensity (RMS(u)o), in this document called I.

CONTROL PARAMETERS ON LARGE SCALE SYSTEM ARCHITECTURE

Clay particles concentration has been recognized as being an important controller in deep water depositional architecture (Wetzel 1993; Reading and Richards 1994 and Covault et al. 2012). Finer-grained sediments feed extensive and larger down-current systems, which facilitates the development of meander channel-levee systems and sheet sands across low-gradient continental floors. On the other hand, coarser grain sizes are associated with higher slope gradient, shorter systems, discontinuity of channel systems and a tendency for such channels to migrate

Following Covault et al. 2012, the architecture of deep water deposits is not only dependent of grain size of the input sediment, but also of the seafloor geomorphology .

Covault et al. 2012, shows a relationship between seafloor geomorphology and length of the system, thus, length is related to relief and the maximum relief of a continental margin is controlled by the tectonic framework (Equation 1 & 2).

$$H = 1034.1 \ln L - 9541.8 \quad (1)$$
$$H = 1071.1 \ln L - 10272 \quad (2)$$

H is relief from canyon head to basin floor, L is length from canyon head to near the point of the channel terminus at the end of the channel-to-lobe transition zone, and ln is the natural lograrithm. First equation is obtained from the relationship between all the author`s data set. The second one is removing three systems, San Antonio (central Chile), Kushiro (Japan), and Aoga (Japan), which developed across tectonically active convergent margins and have greater reliefs for their lengths relative to the other systems

Generally, the authors, besides of corroborating Reading and Richards (1994) work regarding grain-size input and volume of sediment as controllers on systems architecture, added the tectonic setting and intrinsic fluid-dynamics also as important rulers of deep-water architecture systems: The longest canyon, channel systems and largest deep-sea fan with long term, voluminous, mud rich sediment supply are related with mature passive continental margins with large relief from canyon head to channel terminus. Opposite, the shortest, lower-relief canyon and channel systems with short term poor sand-rich or mixed sediment supply are associated with immature margins. In such settings, even if the sediment supply is voluminous, the extension of the system is limited by the basin margins, so that the systems are thick rather than extensive (Covault et al. 2012).

Furthermore, the logarithmic relationship between relief and length can be accounted for intrinsic sediment-gravity flow dynamics. The flow dynamics include velocity (U), with height (h) and concentration (C) as the most important, but also bed roughness, coefficient of clear water entrainment etc. With this work, the effect of the flow dynamics caused by variations in clay content were studied in more detail and give complementary observations to Covault et al (2012) and Reading & Richards (1994) work.

MAIN RESEARCH TOPIC OF THIS THESIS

The study presented here aims to get a better understanding of the effect of clay particles on constant-discharge turbidity flows, with respect to flow behavior and character of its related deposits (particle size distribution, rate of deposition, thickness). This will be achieved by investigating the flow structure in comprehensive sets of Froude-scaled flume experiments never done before.

The main approach is to run a set of experiments with different sediment fraction at a constant sediment concentration of 13% while acquiring high-resolution UVP-velocity (Ultrasonic Velocity Profiler) data and high resolution images when the flow is passing through the flume. This combination gives information about the fluid dynamics of each flow with a particular clay concentration. By comparing the data, the clay effect is investigated with the aim of answering the first two research question: **1.** Does the clay affect the velocity and turbulence profiles in experimental gravity currents? and **2.** Are the five stages from turbulent to laminar flows described by Baas et al. (2009) and Sumner et al. (2009) present in experimental closed-channel flows?

Two additional sets of experiments with constant sediment fraction but different slope angles are recorded (clay at 4% sand at 9% volume concentration (vc) in the first set and 13% sand 0% clay vc in the second set). The aim is to investigate the effect of changing the slope on the grain-size, thickness and sedimentation rates of the associated deposits. With the data acquired in set 2 and 3 the last two questions of this work can be answer: **3.** Following Hofstra (2011) & Gladstone (1998) the addition of small amount of clay will increase even further the transport efficiency of the sand and **4.** Can clean sand packages be deposited from clay-laden flows? if so, what is the depositional architecture of the deposits?

Background

Before Mulder & Alexander (2001) there was a lot of confusion in the field of sediment gravity flows since different processes were named with the same term or there were terms that referred to different processes. Mulder and Alexander (2001) established a simplified classification of subaqueous density flows based on the cohesivity of particles, flow duration, sediment concentration and particle support mechanism (Figure 2). The classification establishes some basis to distinguish between debris flows, hyperconcentrated and concentrated density flows and also turbidity flows. Flows with concentration <9% by volume are called turbidity flows in which turbulence is the dominant particle-support mechanism (Bagnold, 1962 and Mulder and Alexander 2001); Concentrated Density turbidity flows or "high density turbidity flows" as some other authors called them, are flows with concentrations between 9% and around 25-40% (the upper limit cannot be defined as a single value because the threshold volume per cent depends on many factors such as clay content); Hyperconcentrated flows maintain sediment concentration of over 25-40% by volume, and differ from the concentrated flows because of their no-Newtonian behavior. Cohesive flows can hold sediment volumes per cent between 35 and 60%, but the difference with hyperconcentrated flows is that cohesive flows have a matrix strength resulting from the cohesion between particles. Using Mulder and Alexander (2001) classification this study simulates Concentrated Flows since the initial concentration of every run is 13% and Turbidity flows due to water entrainment which makes the flow to evolve to lower concentrations (Figure 2).

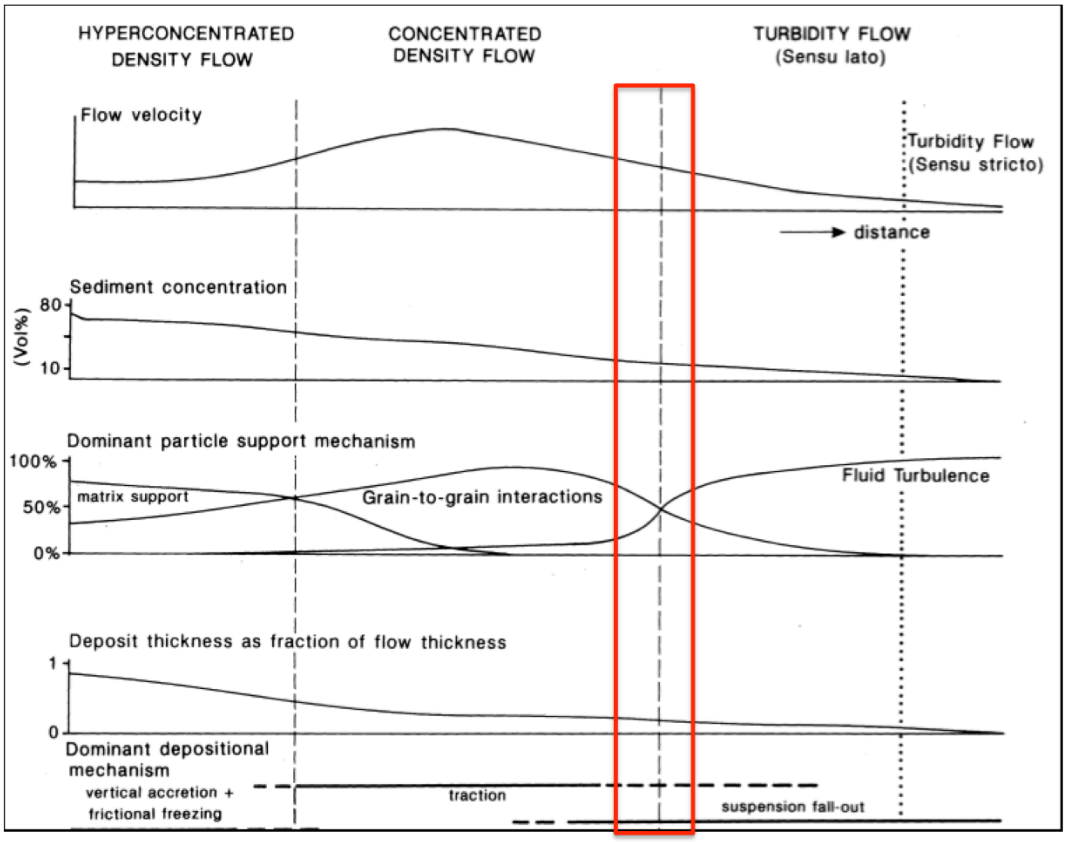

Fig. 2. Curves of the main flow properties in which the classification of marine sediment flows of Mulder & Alexander, 2001 is based: flow velocity, sediment concentration, particle support mechanism and deposit thickness. The red box represents the window in which these experiments are classified.

FLOW STRUCTURE

A turbidity current is divided into three parts: the head, body and tail (Figure 3) (Middleton, 1966, 1967, 1993; Eggenhuisen & McCaffrey, 2009). The head is considered to be a complex part of the current with variable velocities where three resistance forces interact: the ambient fluid resistance, the bed and the upper interface friction. The bed friction produces a "nose"shape at the front and the shear at the upper surface of the head produce turbulent mixing at the back of the head (Middleton, 1993). On the other hand, in the current behind the head, only the frictional resistance is important, producing larger averaged velocities than in the head (Middleton, 1993), this difference in velocities may be associated with an hydraulic jump, and a change in flow properties.

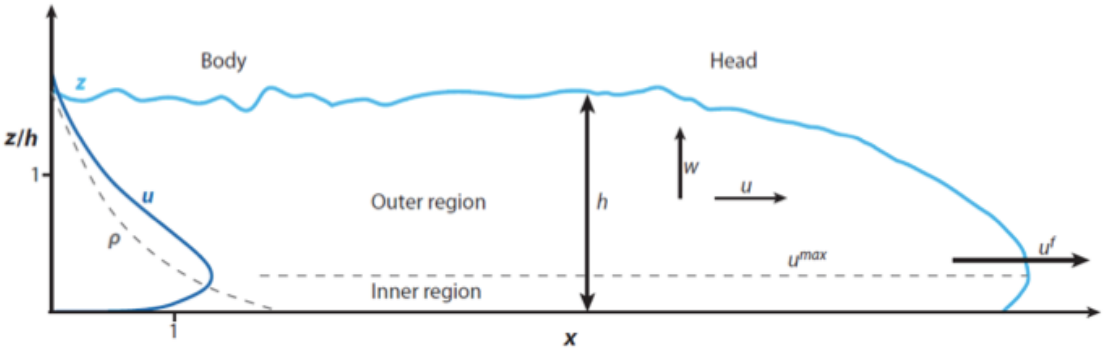

Figure 3. Simplified sketch of a turbidity current showing generalized sediment velocity and density profiles (Meiburg & Kneller, 2010)

It is very important to distinguish between the head, body and tail during the experiments for two reasons: 1) It is common that in laboratory experiments only the body is investigated, thus underestimation of the body velocity can easily happen since the head and tail move slower than the body and 2) to distinguish between the deposits created by the body itself rather than those deposited by the waning phase (the tail).

Velocity Structure

The velocity profile of experimental gravity currents have a typical non-dimensional shape (Figure 4). It consists of an inner region with a positive velocity gradient and properties controlled by the interaction with the underlying bed, and an outer region with a negative velocity gradient and mechanical properties controlled by the ambient fluid above (Meiburg & Kneller, 2010). The inner region is separated from an outer zone by a region of maximum velocity located roughly at the lower quarter of the total flow thickness (Eggenhuisen & McCaffrey, 2012).

Altinakar et al. (1996) proposed two separated functions that represents the velocity in the inner and outer region. A logarithmic function for the inner region and a Gaussian function for the outer area. While the logarithmic function is widely accepted to be a good estimation of shear velocities in the inner region (Kneller et al, 1999; Sequeiros et al, 2010; Xu, 2010), the Gaussian function used to represent the shear velocities for the outer region does not fit with the experimental data, specially with saline currents where the mixing at the interface is suppressed (Gray et al, 2006). Some other authors such us Xu. (2010) suggest that a simple exponential function can better represent the normalized profile of the outer part.

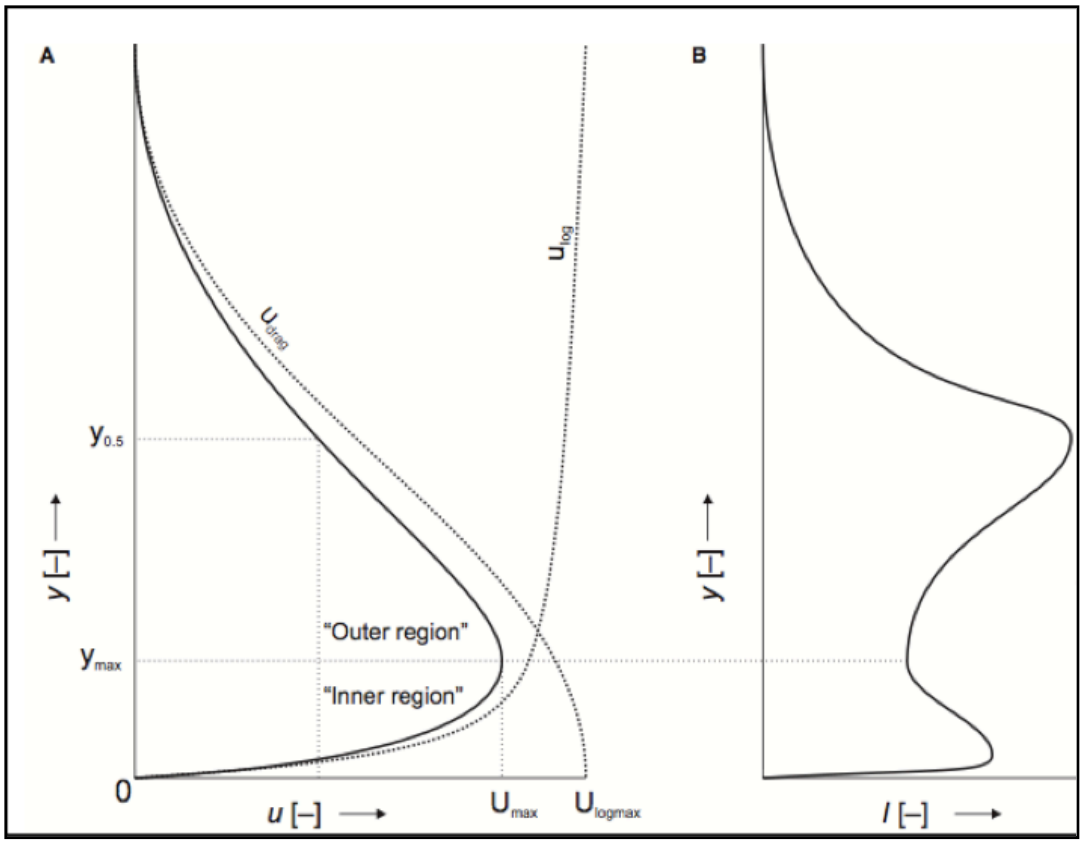

Fig. 4. (A) Idealized dimensionless velocity profile of an experimental gravity current based on a logarithmic function for the inner region and a Gaussian fit for the outer region separated near Umax. (B) Idealized turbulence intensity (Eggenhuisen & McCaffrey, 2012)

Turbulence intensity

The turbulence intensity is a parameter that is largely used in experimental gravity currents (Best et al., 2001; Baas et al, 2009, 2011; Eggenhuisen & McCaffrey, 2012). The turbulence intensity profile of a turbidity current flowing in clean water has its maximum values where the gradient of the horizontal velocity is maximum and shear is largest (Nezu & Nakagawa, 1993). Since the velocity profile has two picks of maximum shear (at either side of the velocity maximum), the turbulence intensity profile should show also two distinctive picks above and below Umax (Figure 4B). Figure 4B is an idealized turbulence intensity profile, but it can also be altered with stratification of the flow.

Methods

EXPERIMENTAL SET UP

Flume tank

The experiments were conducted in the Eurotank Flume Laboratory at Utrecht University. The flume tank used for these experiments has 4m long, 0.26m wide and 0.6m deep and can also be tilted at various angles (Figure 5). The mixture of sand, clay and water was stored in a mixing tank with $1m^3$ capacity. Using a pump the mixture was forced to flow from the mixing tank to the flume. Using a discharge meter the discharge was measured in the pipe that communicate the mixer tank with the flume. In every run the discharge at the pipe was maintain around $58m^3/h$ and $72m^3/h$ although it could reach values up to $164m^3/h$ at the flume as a consequence of entrainment occurring in the flume tank.

When the mixture gets in contact with the flume floor it is pushed out of the inlet. A tilted flat beam is located at the inlet to prevent instabilities of the flow that can be caused by the abrupt entrance of the mixture into the tank. On the flume floor a glued thin layer of fine sand simulates natural roughness and prevents erosion so the flow concentration remains the same. At the end of the flume, the mixture flow into a container attached to the flume tank.

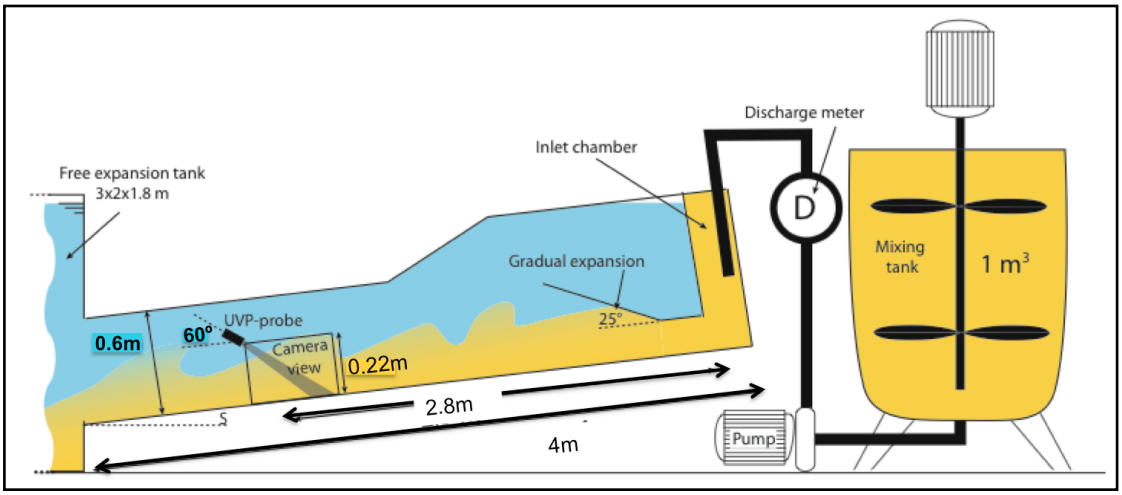

Fig. 5. Sketch of experimental setup. Modified from Cartigny (2012).

Grain size distribution

Eleven successful experiments separated in three sets were conducted using one silica sand and one kaoline clay. The grain-size distribution of three samples of each type of sediment were analyzed with a Mastersizer S long bed Ver 2.18. Figure 6 displays for each sediment component the three-sample average cumulative grain size distribution. The P10, P50 and P90 of the grain-size distribution for the sand are $120\mu m$, $190\mu m$ and $301\mu m$ respectively, and for the clay $1.67\mu m$, $7.7\mu m$ and $41.4\mu m$.

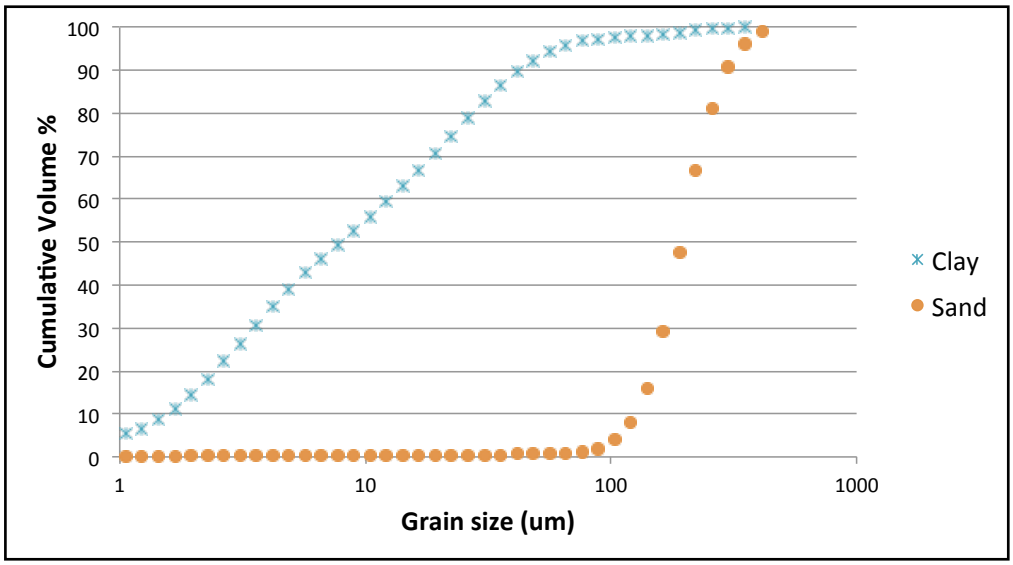

Fig. 6. Total distribution of both type of sediments (sand and clay).

The sediment concentration for all the runs was fixed at 13% volumetric concentration with the proportion between sand and clay being varied (Table 1). An estimation of the moisture of the sediment and thus of the error in the calculated volume, was performed by drying a bucket of clay and a bucket of sand in an oven at 60 degrees Celsius. The moisture in both of the sediments was estimated to be negligible (around 0.75% for the clay and 2.41% for the sand. The last indicates that the calculated weight in kilograms of sediment (clay and sand) that were needed to obtain the certain volume concentration are acceptable.

	Experiment No.	CLAY Fraction %	SAND Fraction %	TOTAL VC %	Slope (º)	SAND Kg/ 800L	CLAY kg/ 800L
SET 1	1	0	13	13	9	276	0
	2	2	11	13	9	233	42
	3	6	7	13	9	148	126
	4	8	5	13	9	106	168
	5	10	3	13	9	64	210
SET 2	6	4	9	13	7	127	84
	7	4	9	13	5	127	84
	8	4	9	13	3	127	84
SET 3	9	0	13	13	7	276	0
	10	0	13	13	5	276	0
	11	0	13	13	3	276	0

Table 1. Overview of all performed runs separated in three sets. 800L of water were used in each run. The density of sand and clay was 2650 kg/m^3 and 2620 kg/m^3 respectively.

MEASUREMENT TECHNIQUES AND DATA ANALYSIS

In all the runs UVP, grain-size and high-speed video data were obtained in order to characterized the fluid properties and the generated deposits. The UVP node was located at a distance of 0.22m above the bedding plane, at 2.8m from the inlet and at 60 degree angle with the bed. At the same location a monochrome camera filmed the turbidity current through the glass side wall of the flume with 210 frames per second. The high speed imaging was used to determine depositional rates, erosive character of the body and general flow behavior in more detail. Sediment cores were acquired in all the runs of Set 2 and Set 3 to perform laser diffraction grain size analysis.

Velocity

The fluid velocities were measured with a single UVP node (See Table 2 for UVP parameter settings). When the UVP node emits an ultrasound pulse and detects the Doppler shift in the reflected signal the velocity of particles in the current are determined (Best et al. 2001). Met-Flow Velocity Profile software was used to record and export the data which consisted on a combination of velocity data (simultaneous velocity data along the axis of the ultrasound beam) as well as the amplitudes of the received signals.

Number of probes	1
Probe height above bed (cm)	22
Probe angle relative to bed (deg)	60
Ultrasound frequency (MHz)	1
Sampling period (ms)	20
Channel distance (mm)	2.78
Channel width (mm)	2.96
Medium ultrasound speed (mm/s)	1.480
Velocity band width (mm/s)	1504.1
Pulse rep. freq (KHz)	2.03252

Table 2. Ultrasonic Doppler Velocity Profiling (UDVP) parameters

To reconstruct the vertical time-averaged profiles of bed-parallel velocities the exported UVP velocity data from Met-Flow Velocity Profile has to be corrected for the inclination angle of the probe. Knowing that the probe is tilted 60 degrees, the significant larger x-direction velocity (v) was obtained by dividing the recorded velocity (V) by the cosine of 60º. It has to be assumed that the main direction of the flow is parallel to the bed and that the vertical movement is only caused by turbulence which results in no net movement (Hofstra, 2011).

Since a turbidity current is divided into three parts: head, body and tail (Figure 3), it was necessary to identify which velocity data corresponds to the body of the current (Figure 7) . Here, the head and the tail were not studied in detail due to their complexity and the few published data available for comparison.

Once the data of the body has been corrected for the UVP angle inclination, the vertical time-averaged profiles are constructed.

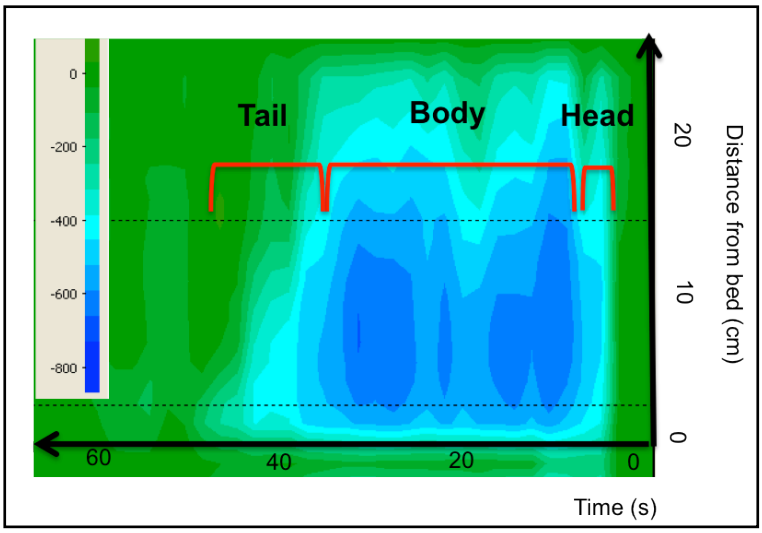

Fig. 7. Exported velocity data from Met-Flow Velocity Profile software. Example of run 2 with 11% Sand - 2% Clay.

Shear velocities

Shear velocities U* was computed using a curve-fitting procedure based on the logarithmic law-of-the-wall (Kneller et al, 1999) (equation 3).

The formula takes into account shear velocity (U*), the vertical position (Z), the von Kármán constant (k) with a known value of 0.41.

$$U^* = k\,(\Delta \ln / \Delta U) \qquad (3)$$

It must be noted that equation 1 is somewhat a simplified equation, and does not take into account Zo, which is the hydraulic (bed) roughness length (Julien, 1998; Carling, 1992).

Simple linear regression of the natural logarithm of the height versus velocity is expected to give a reasonable estimate of the shear velocity. A fit of 95-100% is considered to be valid enough for representing the correct fitting function.

Turbulence intensity

Determining the turbulence intensity profiles is somewhat more challenging. First, the turbulent component of a measured velocity value (v`) was calculated by subtracting from the measured velocity (v) the time averaged velocity ($\tilde{V}$).

$$v` = v - \tilde{V} \qquad (4)$$

Then the turbulence intensity is calculated from formula:

$$I = \sqrt{\sum_{i=1}^{N} \frac{(v_i')^2}{N}} = \mathrm{RMS}\,v' \qquad (5)$$

Where I is the turbulence intensity (m/s) equivalent to the standard deviation of v`, and N denominates the number of data points in the time series for which the turbulence intensity is determined, again only in the body of the turbidity current.

Following Eggenhuisen & McCaffrey (2012) who stated that the time averaged velocity parameter ($\tilde{V}$) can be over-estimated when the turbulence intensity is calculated over a time domain during which the velocity varies; in this work $\tilde{V}$ was computed as a local time-averaged velocity of a moving time-window of 1 second width.

Results

VELOCITY PROFILES

Figure 8 shows the velocity profiles of 5 experiments of set one (note there is no profile for 9% sand and 4% clay) where the effect of the addition of clay on the flow structure is studied.

Despite the fact that the constructed profiles did not go back to zero at the bed, the global structure of the curve shows the main typical characteristics of an ideal velocity profile: a velocity maximum close to the bedding plane and logarithmic distributions in the inner region. The outer part curve does not show a gaussian distribution but this is related with the position of the UVP. Since the node was located at 22cm from the bed and the height of the flows were around 40cm, the curves do not show the most outer values where the gaussian shape is more visible.

At first, for the outer regions the velocities become relatively larger as clay fraction increases, note that for example at run "13% sand-0% Clay" the velocity at 15cm above the bed is around 0.8m/s whereas for run "3% Sand-10%Clay" the velocity at the same location is close to 1m/s. On the contrary, for the inner region the general trend is to obtain a relative slower movement with higher clay concentration, for instance, run "3%Sand-10%Clay" at 2cm above the bed the velocity is around 1m/s whereas for run "3%Sand-0%Clay" is 1.35m/s.

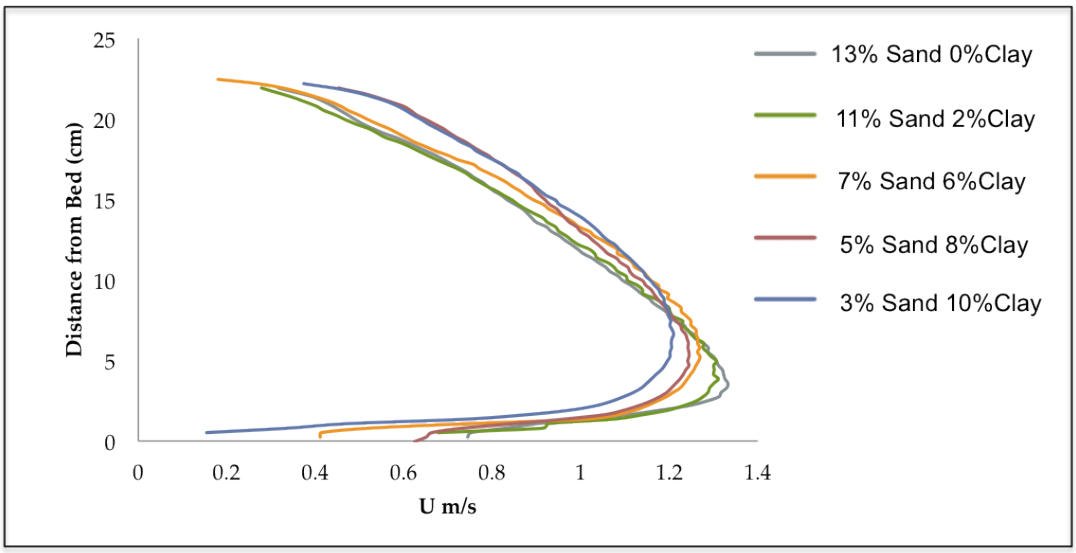

Fig. 8. Dimensional Velocity profiles of the 5 successful experiments of set 1.

Other observations can be made when zooming at the Umax region of all the curves of Figure 8, since the effects of adding different clay proportions becomes even clearer (Figure 9): There is a decreasing trend of Umax as the sand/clay ratio decreases, also the distance between Umax and the bedding plane becomes higher with larger clay fractions (red arrow in Figure 9).

In order to avoid any uncertainties related with dimensional profiles, next section will be focused on analyzing the same profiles dimensionless, so internal shape differences can be better understood.

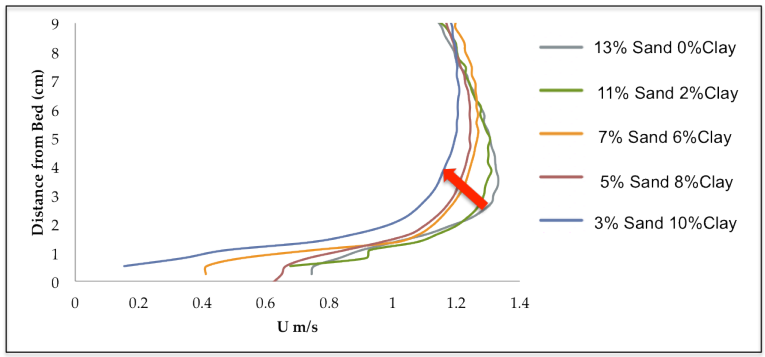

Fig. 9. Dimensional Velocity profiles of the 5 successful experiments of set 1, the red arrow indicates a trend as the clay fraction increases.

Dimensionless velocity profiles

When the velocity data is plotted dimensionless the overall shape of the velocity structure can be analyzed since differences in gradient in the outer and inner region are accentuated. In all the dimensionless profiles the time-averaged velocities of the body are normalized by Umax and are plotted against normalized position H.

Figure 10 shows Figure 8 plotted dimensionless in two different ways. The first one (Figure 10A) has a fixation in the inner part, meaning that Umax was fix at an H value of 1 and therefore gradient differences in the outer region are accentuated. Figure 10B has a fixation in the outer part, with Umax fix at H=0 and Umax/2 fix at H=1, so that gradient differences in the inner region can be studied.

Figure 10A shows that when the clay fraction increases the velocity gradient also increases, and causes the profile to get a sharper shape whereas in Figure 10B, the velocity gradient slightly decreases with higher clay fractions. Also, in Figure 10 B there is a widening of the maximum velocity region giving a more concave shape and a more homogeneous character with greater proportions of clay. Further shear velocity analysis will provide more information about the flow dynamics in the inner region.

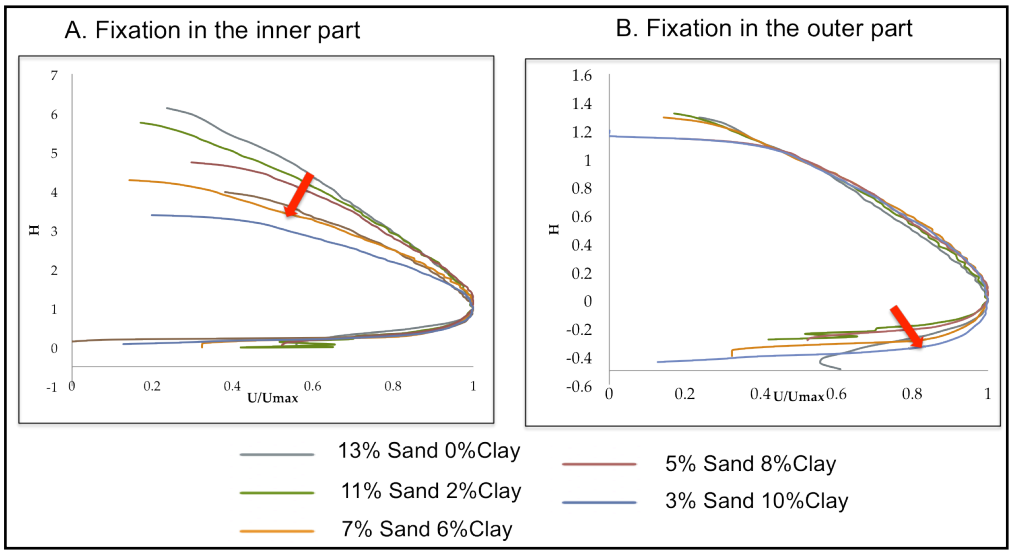

Fig. 10. Dimensionless velocity profiles of the 5 successful experiments of set 1, the red arrows indicate a trend as the clay fraction increases. In B, note that there is an increase in vertical velocity gradient from 13%Sand to 11%Sand, for the rest the tendency is to decrease as it is shown by the red arrow.

Shear velocities approximation

As previously described , the shear velocities have been approximated with the help of the law of wall. This method depends a lot on the quality of the data and caution has to be taken in the interpretation of the results.

Figure 11 shows for each run the linear regression of the natural logarithm of the height versus velocity of the inner region. From these $\Delta \ln / \Delta U$ is determined and then by replacing in equation 1 (note $\Delta U / \Delta \ln$ is present in the equation rather than $\Delta \ln / \Delta U$) the shear velocities were calculated and plotted in Figure 12.

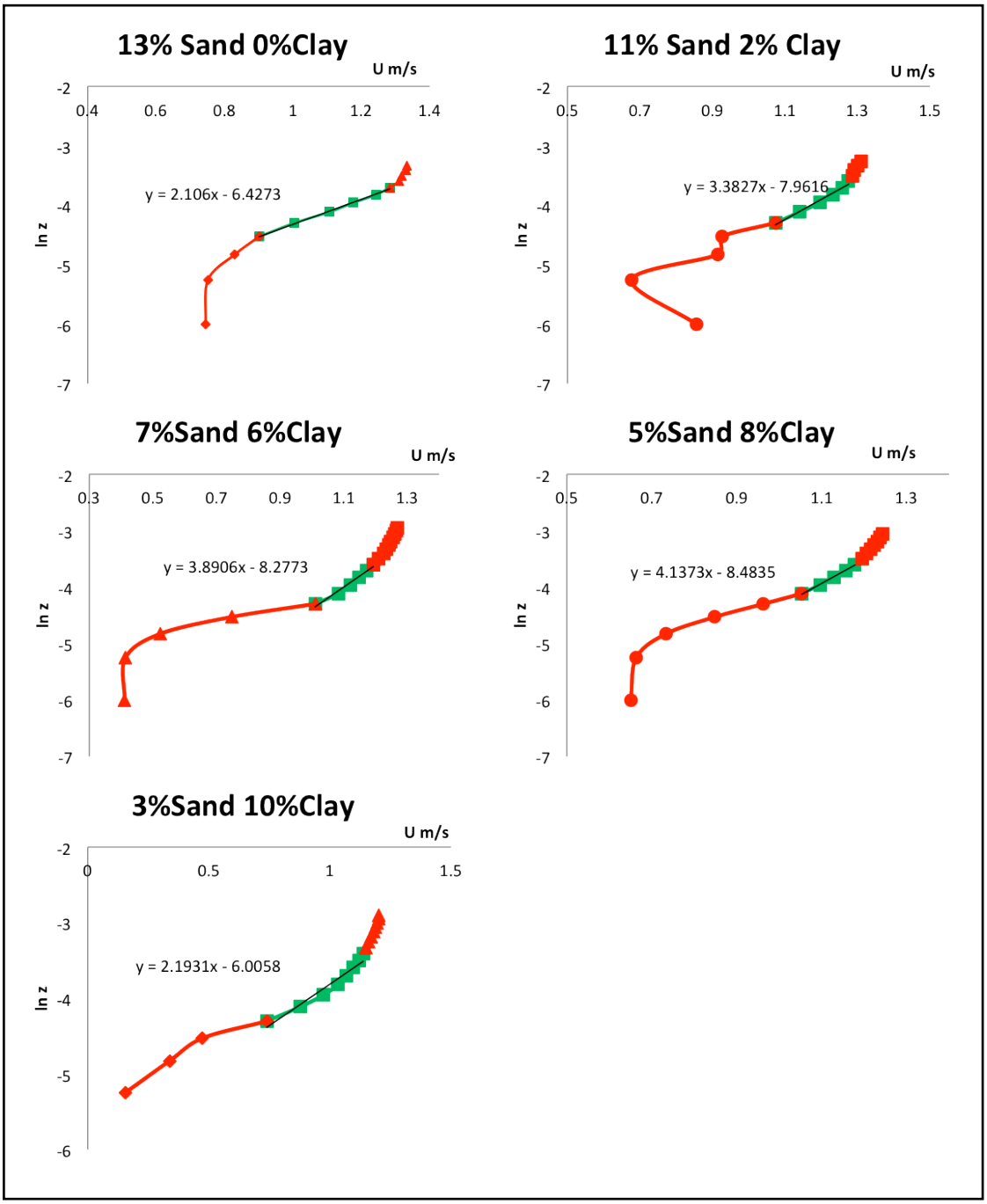

Fig. 11. Linear regressions of the natural logarithm of height vs Velocity of the 5 successful experiments of set 1, the red points were not taken into account for the regression since they show anomalous trend caused by acquisition problems at the base and maximum velocity disturbance at higher heights.

As it is shown in Figure 12 there is a clear relationship between shear velocity and clay concentration. With higher clay content the shear velocity tends to decrease. Run with 10% Sand 3%Clay seems to be an exception to the pattern mentioned before and can be related to an experimental error.

Nezu & Nakagawa (1993) demonstrated a relationship between stream wise velocity and shear velocity for open channel flows, by having a ratio between the both of 2. In this work this ratio is between 1.2 and 1.5, the difference with theoretical value can be due to the fact that closed-channel currents can behave differently and also because the data quality in the inner area is very low. Despite the difference in ratio between stream wise and shear velocities, the data plotted in Figure 12 gives new insights into clayey closed-channel flows.

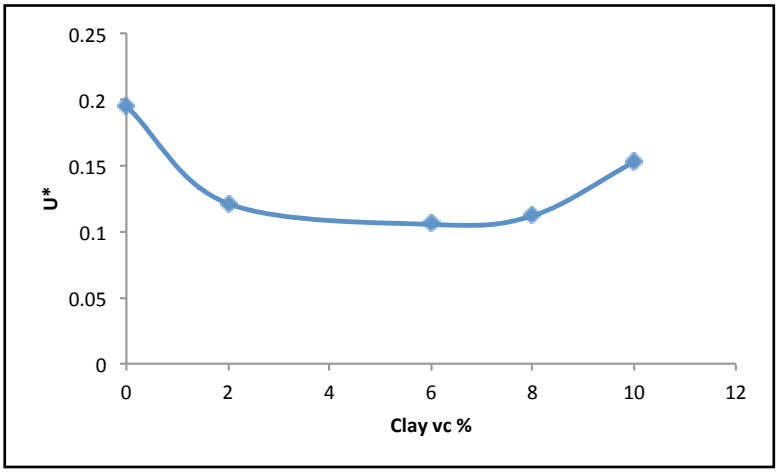

Fig. 12. Shear velocities of the five successful experiments of set 1.

TURBULENCE INTENSITY PROFILES

Figure 13 compares the profiles of vertical turbulence intensities of runs from set1. For all five runs, there is a lower turbulence maximum below 2cm from the bed and a turbulence minimum close to 3cm. The position of the upper turbulence maximum is around 15cm only for runs with 5%Sand-8%Clay and 3%Sand-10%Clay. For the other runs the position of an upper turbulence maximum is not clearly discernible since there are two picks with large turbulence intensity.

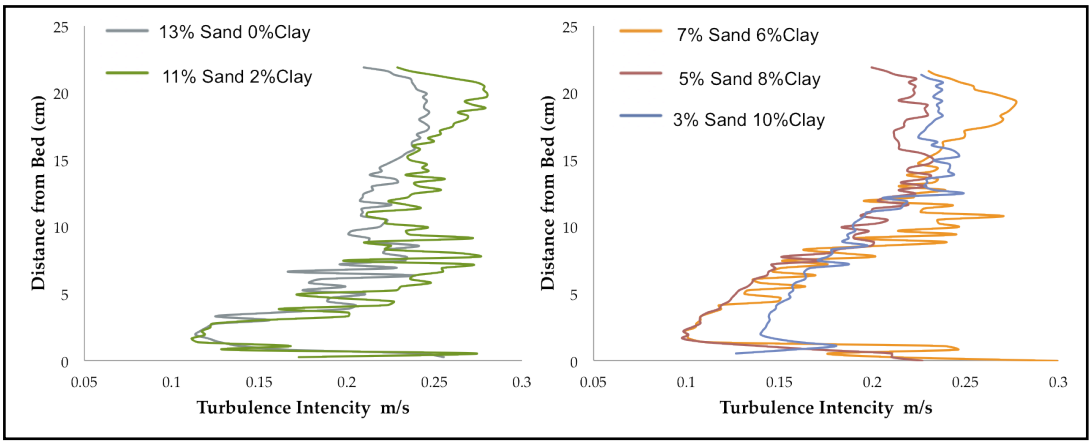

Fig. 13. Turbulence intensity profile of the 5 successful experiments of set 1.

As it is shown in Figure 13, the small addition of clay (from 0%Clay vc to 2%Clay vc) causes the entire profile to shift to higher turbulence intensity values. From clay volume concentrations equal or higher than 6% the evolution of the profiles is different for distances from the bed lower and higher than 10cm. For instance, the profiles with 6% and 8% clay vc, move to lower turbulence intensities only at lower distances from the bed, whereas at higher distances from the bottom the profiles show relatively higher intensities than runs with 2% clay vc.

The run with most clay vc (blue profile) shows a distinctive increment in turbulence intensity along the entire turbulence intensity profile. This profile is somewhat of an exception, and can be related to experimental error, as it was mentioned observed also in Figure 12.

The position above the bed and intensity of the lower turbulence maxima are shown in Figure 14 A and B, respectively. The position of the maximum goes up with increasing clay content, when the clay vc reaches 8% the lower maximum shifts closer to the bed, at 10% clay vc, the height of the maximum increases. This last increase in height with maximum clay vc is somehow unreliable since as it was mentioned before, this run can be related to an experimental error.

The intensity of the maximum increases with increasing initial clay volume concentration from 0% to 2%. Above 2% clay vc the intensity of the maximum decreases linearly.

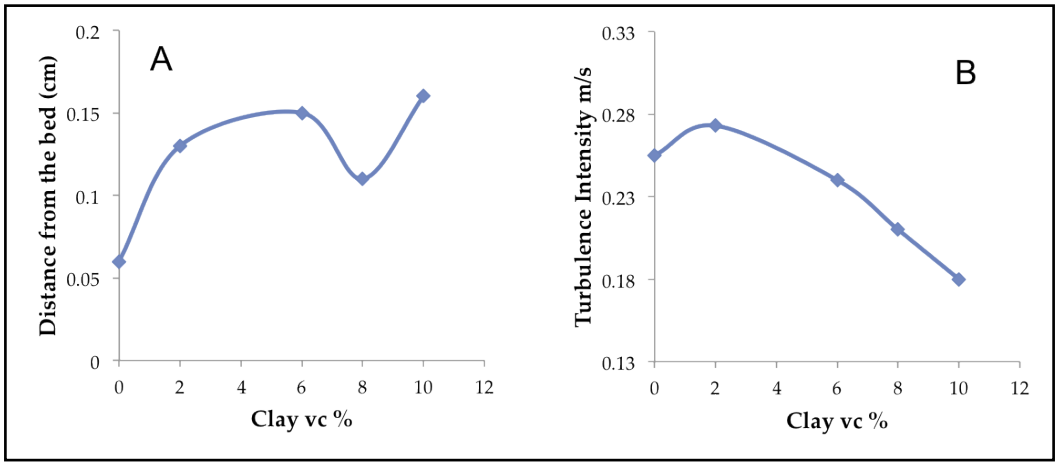

Fig. 14. A. Height of the lower turbulence maxima of experiments of set 1. B. Intensity of the lower turbulence maxima of experiments of set 1.

Normalized turbulence intensity profiles

In Figure 15, the profiles of the turbulence intensities for runs of set 1 are normalized with Umax and are plotted against H (with Umax fix at H=1). In this way, the turbulence values in the inner part can be studied in more detail. The small addition of clay causes the lower maximum normalized turbulence to increase 2% (passing from point 1 to point 2 in Figure 13) and also to shift the vertical position of the maximum higher up around 0.15. With the subsequent extra addition of clay by 4% vc the lower normalized maxima decreases (points 2 to 3) till 19.5 and also moves slightly further from the bed till 0.2. From point 3 to 4 extra 2% of clay caused the lower normalized maximum to decrease by 2.5% and to move down its location in the vertical again at

0.1. Finally with a final clay vc of 10% the lower normalized maximum decreases dramatically and shifts again away from the bed till 0.2 (point 4 to 5) .

Note that this plot is highly in accordance with the observation made from Figure 14. This is showing the consistency between dimensional and normalized data.

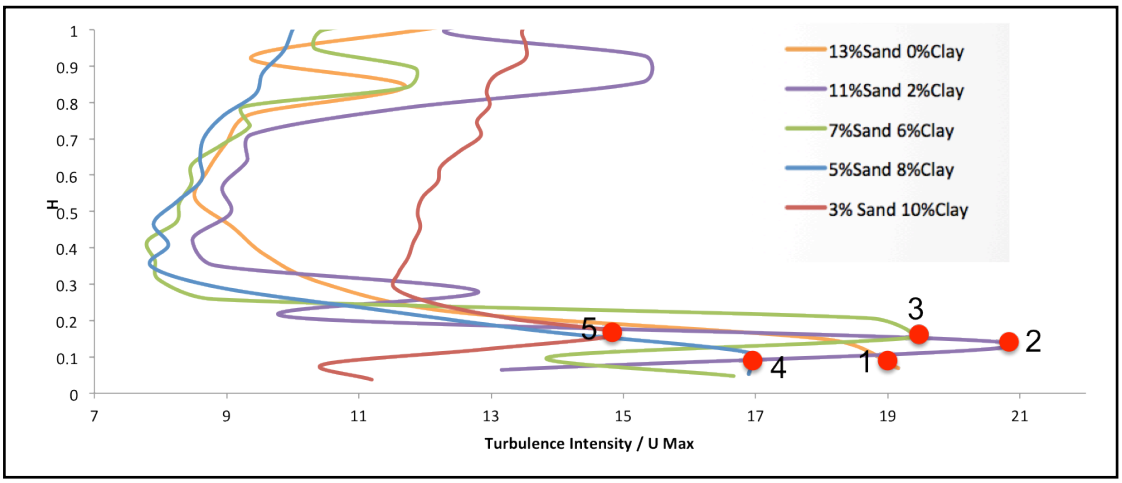

Fig. 15 Turbulence Intensity of the inner area of flows of set1. Lower maximum turbulence intensities represent in red dots with numbers denoting a gradual increment of kaolinite.

It is very important to mention that due to the position of the UVP which was located far from the bedding plane, all the observations made for the inner part of the flow have to be taken with extremely care since the data quality in this region is often very low.

CHARACTERIZATION OF DEPOSITS OF SET 2 AND 3

Using the velocities images from the UVP software (Figure 7) one can determine the duration of the body and the tail in each run, and thus capture each length in the video camera data to calculate the thickness and sedimentation rates of the sand-body and sand-tail deposits. Besides the distinction of the flow parts was vital to perform the sampling of the deposits for the grain size analysis. Roughly the head of the flow lasted around 5 seconds, the body around 30-35 seconds and the tail 20-25 seconds, resulting in runs of a total length of around one minute.

Sedimentation rates and thickness of the deposits

Figure 16 and figure 17 show the thickness and sedimentation rates plotted against slope. The samples were taking in both tail and body deposits in order to make comparisons between the both. Note that there is not sand body-deposits at 9 sand fraction, thus for this experiments the body of the flow was by passing even at the lowest tested slope of 3 degrees.

The thickness of the deposits in the laboratory were controlled by both slope angles and sand:clay ratio (Figure 16). There is a general increase in thickness as the slope decreases, specially for the deposits created by the body at 13% sand sediment concentration, in this case the thickest deposits, around 60mm of pure sand, occur at slopes of 3deg, whereas no sand-body deposition occur at 9 deg (bypassing slope).

Also, when comparing deposits at the same slope but different input sediment fraction, the results displayed that thickness decreases dramatically with the addition of clay. The tail deposits with 13% sand sediment concentration are nine times thicker than 9:4 input concentrated tail deposits.

Furthermore, there is a large difference in thickness between the body and the tail deposits when comparing them at the same slope, bodies are around three times thicker than the tail related deposits.

The thickness distribution of the tail deposits in muddy flows is rather constant, specially at 6deg where there is a remarkable flat plateau. This trend can be related with the presence of clay particles in the parental flow.

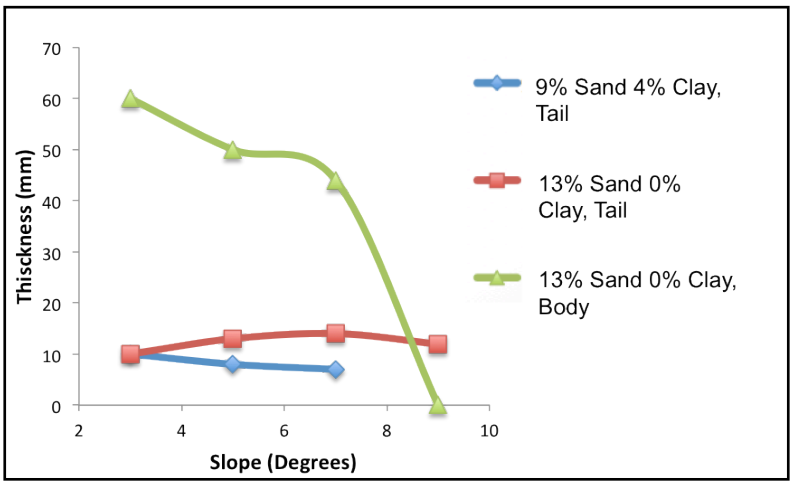

Fig. 16. Thickness variation of deposits of set 2 and 3.

The sedimentation rates are also strongly influenced by grain size input. In flows with clay particle volume concentration of 4% the sedimentation rates were minimum (between 0.4 and 0.5 mm/s) (Figure 17). The rates of deposition of clay-free laden flows are at least twice larger than for muddy flows (between 1 and 2mm/s).

Besides, sedimentation rates also get higher with lower slopes, both for tail deposits and body deposits, and in general tend to be higher for body deposits than for tail sediments.

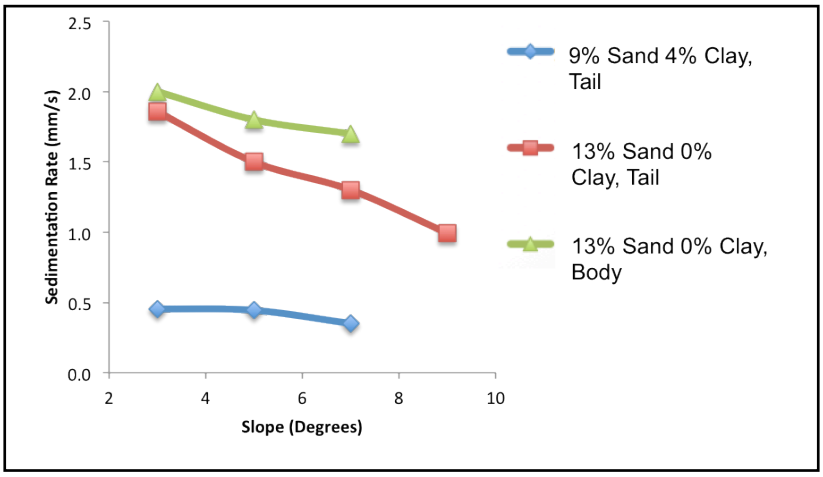

Figure 17. Sedimentation rate of deposits of set 2 and 3

It is important to mention that the discharge was in general maintain between 58m^3/h and 72m^3/h. Therefore, any effect of variation in the settling rate between experiments can be associated to the studied parameters, slope angle and composition of the sediment input, rather than to experimental set-up interferences.

Grain size distributions

Figure 18 shows the grain size particle distribution of the tail and body deposits created by pure sandy mixtures flowing on two different tilted floors (5 Degrees on the left and 7 degrees on the right). The input sand distribution was also plotted to compare with the sample distributions.

The data can be separated into three distinguishable families: 1. The parent input sand in orange, 2. Tail deposits in blue and 3. Body sand deposits in red. The distributions are always coarsest at the body deposits (P50 = 220μm) and finest at the input sediment (P50 = 190μm), the tail deposits (P50 = 205) are in between these two. There is a difference of 15um between each family, indicating an increase of 7% P50 grain size between families.

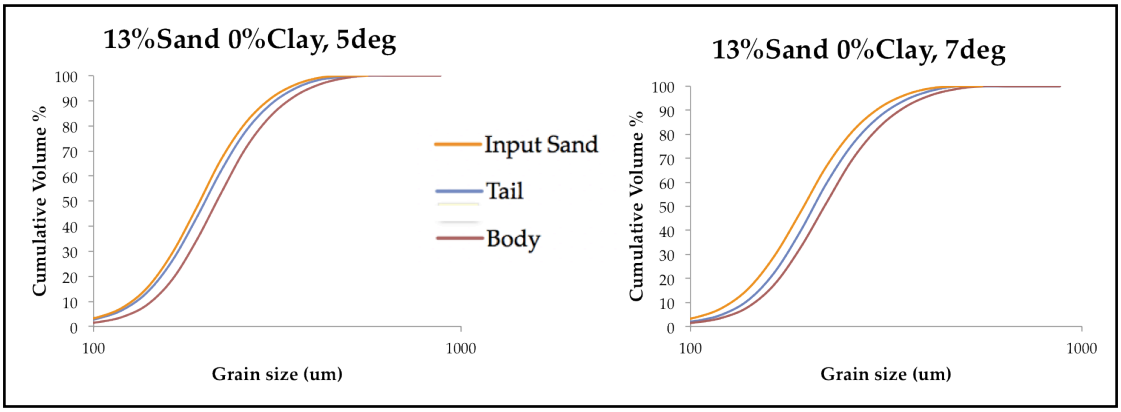

Fig. 18. Grain size distributions for all the deposits of set 2 and 3.

When comparing only the curves of the tail deposits, two important observations are recognized: the grain-size distribution of tail deposits are independent of slope angle (Figure 19) and clay input (Figure 20).

The distribution of grain-size particles of only tales is independent of slope (Figure 19) . All the curves have a very similar trend, even when the graph is zoomed in the distribution remains quite similar. As it is illustrated in Figure 19.B, the P50 for tail deposits are between 205μm and 210μm, which is a very narrow range which restrict the mean grain size particles of the tail deposits. Another important characteristic of tale deposits created by clay-laden flows, is that the sand deposits are extremely clean, less than 2.5% cumulative volume has a grain size particle smaller than 50μm (Figure 19C).

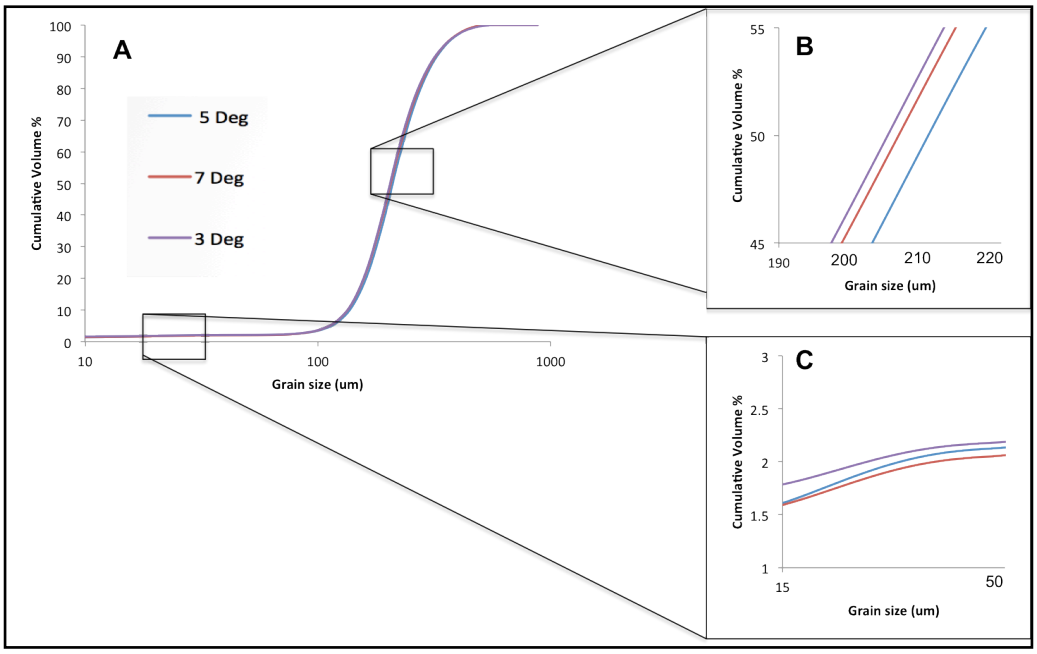

Fig. 19. A. Grain size distributions of the tail deposits created by a flow of 9%Sand - 4%Clay VC at different slopes. B Plot zoomed-in at P50 cumulative volume concentration . C. Plot zoomed-in at grain sizes between 25 and 50μm.

Figure 18 shows all the grain size distributions of all the deposits of set 2 and 3. The grain size distributions of tail deposits are also independent of the addition of clay in the flow as it is shown by the similar distribution of all the blue curves.

For the body deposits (red curves), there is also an independence of slope angle, again they all have the same grain size distribution. However the relationship with clay input is beyond the scope of this work since as it was mentioned before, the set of 9%Sand-4%Clay did not generate body sediments even at the slowest slope tested (3 Degrees) and thus there was not data for comparison.

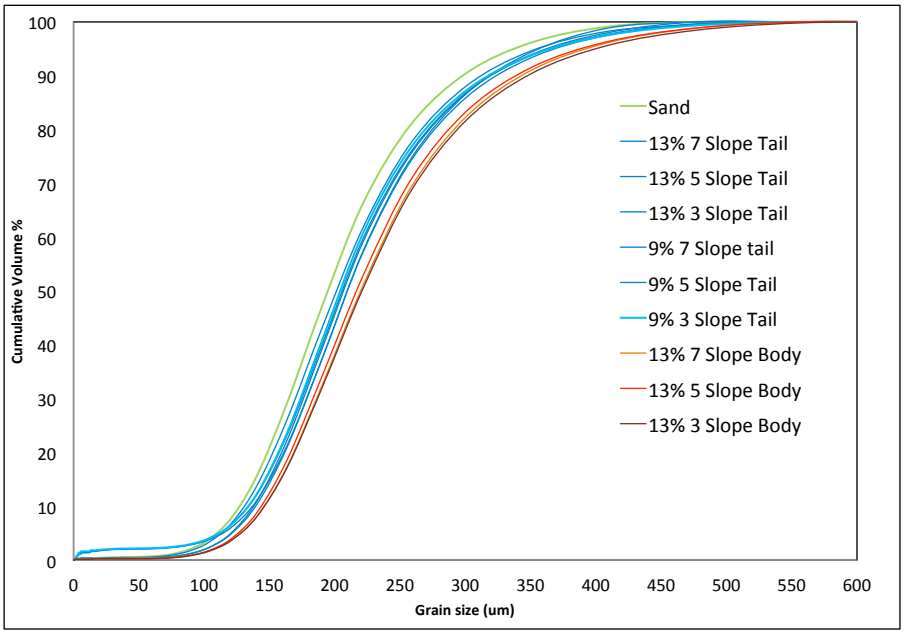

Fig. 20. Grain size distributions for all the deposits of set 2 and 3.

SUMMARY OF RESULTS

The outcome of the first set showed a clear relationship between clay concentration and velocity. Dimensional plots, show that the addition of clay cause the velocity at the outer region to become relatively larger than in pure sandy flows, whereas in the inner region the velocity decreases. Also the Umax becomes lower and furthest from the bedding plane with larger clay contents. The dimensionless plots indicates an increase in velocity gradient with higher clay fraction for the outer part, whereas for the inner part the velocity gradient decreases with the addition of clay. The shear velocity is also affected by the addition of clay, larger shear velocities are associated with small clay content whereas small shear velocities occur in muddy flows.

The turbulence intensity in the outer part of the flow tends to increase with small addition of clay (only 2%Clay) but in later stages the intensity increases. For the inner part of the flow, the turbulence intensity increases with the first addition of clay and after it decreases dramatically.

All the observations made for the inner region have to be taking with extremely care since the resolution in this area is low.

The outcome of the second and third set, shown that the thickness and sedimentation rates are strongly influenced by the addition of clay and the slope angle. There is a general increase in thickness and sedimentation rates as the slope and clay content decrease.

When comparing the grain size distribution of all the deposits, it is always evident that the sand body deposits are coarser than the tail deposits and at the same time the tail deposits are always coarser than the input sediment. Furthermore, the distributions of the tail are independent of slope angle and clay content, whereas the body was only probed to be independent of slope. Clean packages of sand were found in the tail deposits of a muddy flow (9%Sand vc- 4%Clay vc). None of the body deposits were created under muddy flows not even at the lowest tested slope of 3 degrees.

Discussion

The data acquired in this work can give several new insights about internal fluid dynamics of density flows, specially of concentrated flows or High Density Turbidity Flows. Also, information about the character of the associated deposits can be complementary for the classification of turbidity systems such as the ones from Reading and Richard (1994) and Covault et al. (2012). Since the internal processes in concentrated flows can be very complex and not direct data can be compiled from outcrops, seismic or well logs, experimental studies are urgently needed to understand the flow-dynamics and its expression in the sedimentary record.

The following discussion contains two main topics: 1. Clay effects on fluid dynamics and 2. Clay effects on sand deposition and on large scale system architecture.

1. FLUID DYNAMICS

Experimental set 1 was designed to investigate the effect of clay particles on two specific fluid dynamics: Velocity and Turbulence. Also the results were compared with the data of Baas et al. (2002, 2008 & 2009) from open-channel flows and with data from Hofstra (2011) who studied the effect of silt (D50 of sediment used by Hofstra = 50μm) in experimental High Density Turbidity Currents.

Velocity and Turbulence

Since the discharge, slope and sediment grain-size of the sediment input was kept constant for all the runs the only reason for any variation in flow dynamics can be attributed to the clay addition. From the observations made from Figure 8 to Figure 15, the first research question stated here "Does the clay affect the velocity and turbulence profiles in experimental gravity currents?" can be answered by stating that the fluid dynamics of turbidity flows are strongly influenced by the addition of clay particles in the flow. This statement is support by the fact that there is a decrease in Umax, a generation of a blunt-nose, a decrease in velocity gradient in the inner part and an increase velocity gradient in the outer part with the addition of clay. Also there is a general trend to obtain lower shear velocities and lower turbulence intensities with higher kaolinite concentrations in the inner region and a general increase in turbulence intensity for the outer part of the flow. Following discussion will be focused on the analysis of each of the mentioned effects that kaolinite had in these experiments.

The decrease in Umax can be associated with the properties of the clay itself. Since the interaction between clay particles via Van Der Waals attractions become stronger with higher clay concentrations, this interactions make the fluid behave as a Non-Newtonian fluid (Maciel et al. 2009, Coussot 1995). In non-Newtonian flows the fluid exhibits a yield stress ($\mathcal{T}$c), which needs to be overcome for flow to take place. This $\mathcal{T}$c increases rapidly with particle volume concentration (Coussot 1995). At very low clay concentrations the clay particles are distant from each other and thus the yield stress is lower, as the clay particles become more abundant the spaces between each other are reduced and stronger interactions take place, this can lead to a considerable reduction in velocity since the fluid needs more energy to overcome $\mathcal{T}$c.

The bluntness of the nose is a direct consequence of the effects that the addition of kaolinite produce in the inner region of the flow. When looking at the dimensionless velocity profiles, the curves show a widening of the maximum velocity region with a

more concave shape and a more homogeneous character with greater proportions of clay. This is due to the inability of the local shear stresses to maintain a steep velocity gradient as the clay content increases. Figures 12, 14 and 15 supports this idea by showing a reduction in shear velocities which causes a decrease in turbulence intensity and thus a lower velocity gradient (bluntness) with the addition of kaolinite.

In the outer region the velocity and its gradient together with the turbulence intensity increase with higher clay content. The last observations can be related with the amount of water entrainment in the moving flow: Kaolinite particles will cause the flow to expand largely when it enters into the flume causing strong interactions with the clear water above it and subsequently generate higher water entrainment. This entrainment results in larger flow velocities and turbulence intensities in the outer part of the flow.

As a final remark, the vertical distribution of the clay in muddy flows can also be studied. For instance, in run 11%Sand 2%Clay, the clay must be concentrated in the inner part of the flow since here the velocity gradient, Umax and turbulence are low, and in this study these are effects associated with the presence of clay. On the other hand, in the outer part of the flow where the velocity gradient and turbulence intensities are high, the kaolinite concentrations are diminished by dilution caused by the entrainment of clear water.

Transition from turbulent to laminar flows in subaqueous sediment density flows compared to open channel flows

These experimental data represent closed-channel flows, in which small changes in the amount of clay concentration causes remarkably variations in velocity and turbulence intensity. Since past experimental investigations have been focused on the effects of clay particles in flow-dynamics of open-channel flows (Wang and Larsen 1994, Wang and Plate 1996; Baas, Best 2002, 2008 and Baas et al. 2009) rather than closed-channel flows, this work was intended to make a comparison between the fluid dynamics of both kind of currents.

Early models for open channel flows assume a gradual turbulence damping as the concentration of sediment particles increases (Mulder and Alexander 2001, Winterwerp and Van Kesteren 2004). However, after Wang and Plate (1996), Baas and Best (2002, 2008), Baas et al. (2009) , Sumner et al. (2009) and Talling et al (2012) the fluid dynamics of muddy open-channel (at least for the inner part of the flow) has started to be discussed as a more complex interactions between clay particles (cohesive forces) and shear stress (turbulence generator). Depending on which of this modulators preserves the flow will fall in one of the five distinctive flow-phases defined by Baas et al (2009): Turbulent flow, turbulence-enhanced transitional flow, lower transitional plug flow, upper transitional plug and quasi-laminar plug flow (Figure 1) .

In the turbulent flow phase from Baas et al (2009) the downstream velocity is characterized by a logarithmic profile and the normalized turbulence intensity by a gradual decrease as height above the bed increases. From Figures 9 and 15 the same characteristics are recognized in run 13%Sand 0%Clay. Also the lower maximum turbulence of this run is localized at a distance of only 0.6 cm above the bed (note is the closest maximum to bed of all the runs of set 1, Figure 14A), suggesting that the lower maximum turbulence is related only with the shear stresses at the near-bed boundary and not with a free shear layer within the flow.

In the turbulence-enhanced transitional phase of Baas et al (2009), velocity decreases and the normalized turbulence intensity increases by a 17%, this increment in turbulence might be due to the development of a near-bed internal shear layer, as it is suggested by the authors. In this work, run with 11%Sand and 2%Clay also show the same decrease in velocity and increase by 10% in the normalized turbulence (Figure 9 and 15). This run is the only one that has an increment in the velocity gradient and represents the point where the maximum near-bed dimensionless normalized turbulence intensity is present in closed-channel flows (Figure 10) .

The next phase produced by increasing the clay content as it is defined by Baas et al (2009) is the Lower transitional plug flow. In this phase there is a larger increase in turbulence intensity near the bed, these flows can reach up to 65% higher turbulence intensities than turbulent flows. At the top of the flow ("top" meaning closest to the maximum velocity, and not the top of the flow), the normalized turbulence decreases since cohesive forces start to act, and start to develop a plug flow. In this work, these phase was not recognized. None of the runs have an increase in turbulence intensities near the bed while having a decrease in turbulence near the velocity maximum (Figure 15).

In upper transitional plug flows the near-bed velocity continues to decrease and the dimensionless turbulence intensity decreases in the entire flow and the lower maximum turbulence intensity shifts away from the bed. The run with 7%Sand and 6%Clay represents very accurately these changes in the flow dynamics (Figure 14 and 15). Finally under conditions of quasi-laminar plug flow, the velocity, turbulence intensity and normalized turbulence intensity continue to decrease, since the yield stress within most of the flow is very high and damps any turbulence, except near the bed where some bed--shear stresses are still generated. In this work the run 5%Sand 8%Clay matches finds parallels in the trends found for Baas et al (2009).

The run with maximum clay content (10% Clay volume concentration) is considered here to be a non reliable experiment, since it falls out of of all the trends that were identified in the turbulence intensity, lower turbulence maxima position and normalized turbulence intensity (Figure 13, 14 and 15). However, by taking into account the effect that clay has on suppressing the turbulence, this run should have shown even lower turbulences through the entire profile since the clay content was maximum.

From the last discussion the second research question stated here can be answered, **2.** Are the five stages from turbulent to laminar flows described by Baas et al. (2009) and Sumner et al. (2009) present in experimental closed-channel flows?. The effect that clay has in closed-channel flows are quite similar to the ones caused in open-channel flows, and so at least four of the phases from turbulent to laminar flows can be distinguished.

Flow phase diagram

Figure 21 shows the data from this work plotted on the phase diagram of kaolinite-water flows from Baas et al. (2009) together with the data of Sumner et al. (2009). Baas et al (2009) plot a boundary on the left hand side of Figure 21 that separates currents that will generate clay deposits on the right side from non depositional flows on the left side. Most of the data from these study fall on the clay deposition area, and somewhat matches with the trend of the boundaries between turbulent, transitional and

laminar flow phases. Consequently, with the new data presented here the boundaries can be extended to lower flow velocities.

The data from Sumner et al (2009) is shown in black dashed lines and represent an expansion of the work of Baas et al (2009) by incorporating flows that contain also sand. As it is expected, with Sumner et al (2009) data, it is experimentally confirmed that the deposition of the sand begins at much higher flow velocities than for clay. Despite the fact that the boundaries in between the phases plotted by Baas et al (2009), Sumner et al (2009) and the data presented here, do not exactly match, the trends of all the experimental data are very consistent by indicating fluctuations in shear velocities as mud content increases. Differences in grain sizes, composition, bed-roughness and set-ups, used by each author might be the reason for mismatches between the phases boundaries.

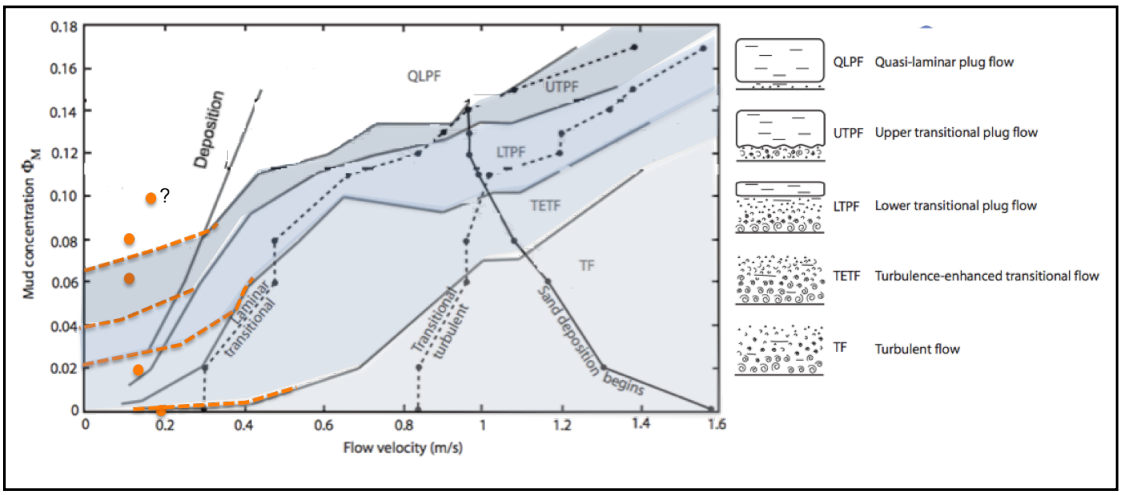

Fig. 21. Data from this study (orange lines and dots) plotted on phase diagram for kaolinite-water flows (grey lines) from Baas et al (2009) and data from Sumner et al (2009) in black dotted lines.

It is important to mention that the results of these experiments should however be taken as a first insight into the investigation of the effects of clay in flow dynamics of subaqueous flows. Meanly the outcome data of the inner part is only a general, qualitative result since the resolution in this part of the flow was low. Further research has to be done in order to confirm these first preliminary results.

2. EFFECTS OF CLAY PARTICLES ON SAND DEPOSITION

The following discussion will be centered on the analysis of the results of set 2 and 3. By comparing the associated deposits of sandy flows with the ones generated from muddy flows, the effects that clay has on the depositional behavior of subaqueous flows , on system architecture and facies distribution is discussed in the next subchapters.

Stability field for sand deposition

From the results of set 2 and 3 (Figures 16 to 20), essential information is obtained about the depositional behavior of the current. Runs of set 2 were all non aggrading: the flows with 9% sand 4%Clay volume concentration, and slopes of 9,7, 5 and 3 degrees, did not generate any body deposits. On the other hand, runs of set 3, were in majority depositional: Only the current with 13%Sand 9%Clay volume concentration at 9 degrees slope had a bypassing body-flow, whereas at slopes of 7, 5 and 3 degrees aggrading body-flows generated considerable thick packages of sand (Figure 16 and 22).

The transition between aggrading and non-aggrading behavior is a function of sediment fraction (Figure 22). The increment in clay content causes the equilibrium slope to decrease, indicating the ability of kaolinite to maintain sediments in suspension and restrict the deposition of sand even at very low slopes. This effect can be accounted to the follow reason: Lower settling rates of particles are expected in flows with higher viscosities. Since clay-water mixtures are more viscous than pure water fluids, clay-laden flows have lower settling velocities and thus are more efficient on transporting sand particles.

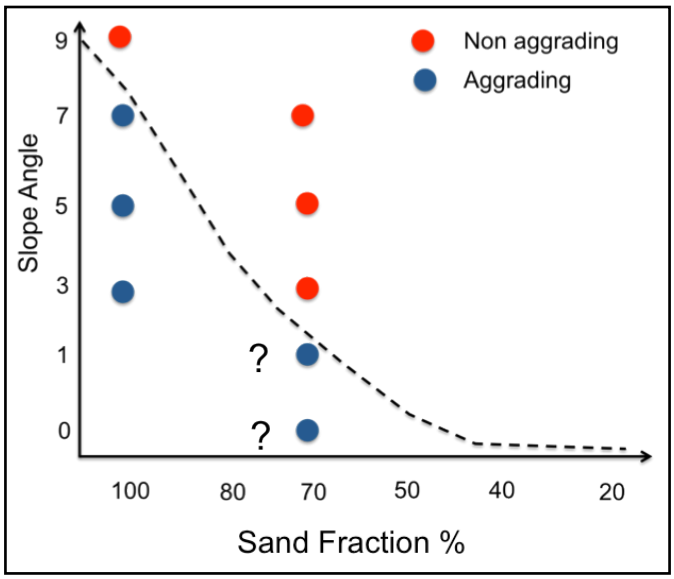

Figure 22. Stability diagram of results of set 2 and set 3 with an interpreted equilibrium line between aggrading and non- aggrading conditions.

The fact that clay is able to hold coarse grained particles in suspension suggests that the transport efficiency of muddy currents is larger than in sandy flows. Gladstone et al. (1998), concluded that in flowing mixtures that contain a small portion of *fines* also the coarse-grained particles will travel larger distances before settling. So, the question

that comes out is: Which of the fine particle enhances more the carrying capacity of the flow: clay or silt.

When comparing the results obtained here with the ones of Hofstra (2011) and Cartigny (2012) (Figure 23), it becomes clear that the addition of clay forces the system to reach lower equilibrium slopes than the addition of silt. Hofstra (2011) found that pure silty flows (blue dashed line) with a 13% Sediment concentration have a bypassing slope at 6 Degrees, here, with the addition of only 4%Clay vc in the flow the bypassing slope was lower than 3 degrees angle.

Important to mention, is the fact that the pure sandy flows in this work have a lower equilibrium slope that the 100% sand concentrated flows of Hofstra (2011) and Cartigny (2012). This can be attributed to the fact that these experiments were performed using higher discharges (58m^3/h and 72m^3/h) than the ones of these authors (Hofstra, 2011 used 9.5m^3/h and Cartigny, 2012 used 2.6 dm^3/s). Also differences in the sediment grain size and set up can produce important differences.

Despite the differences in the angle slope, the comparison is still valid. As it is shown in Figure 23 the dramatic decrease by at least 77% between the bypassing angle slope of sandy currents and bypassing slopes in clayey currents is very remarkable, taking into account that only 4% of clay was added. Besides, the decrease in the equilibrium slope in Hofstra`s data is of only 45% between 100% sandy flows and 100% silty currents.

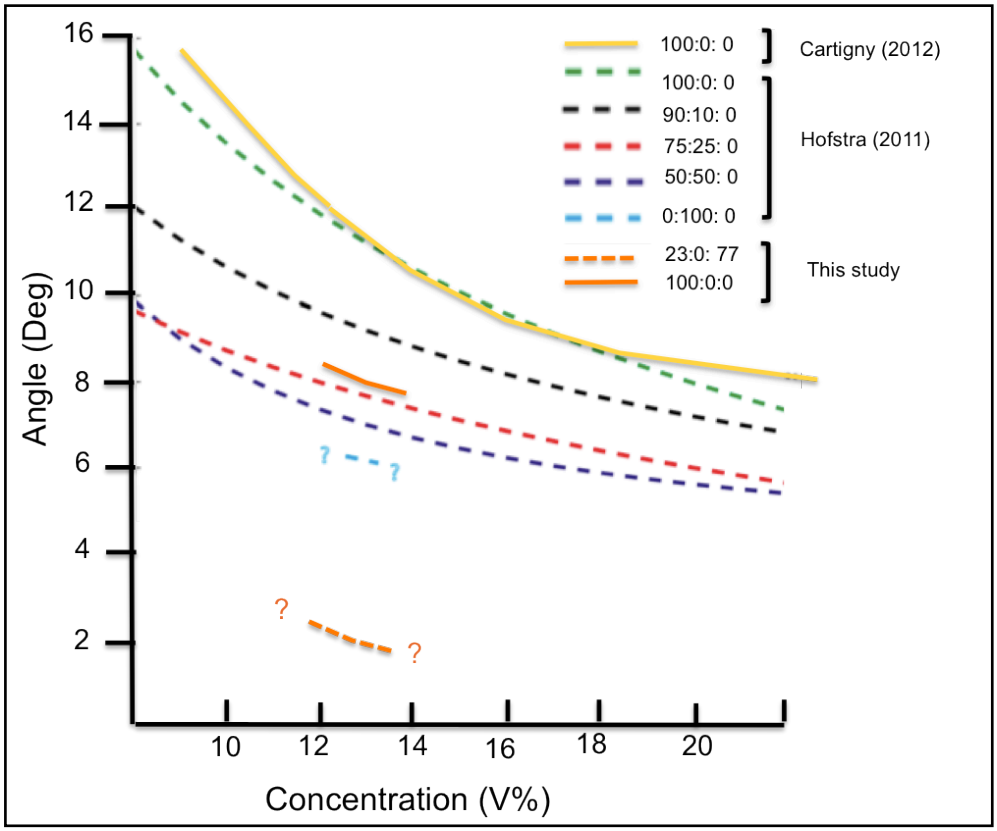

Fig. 23. Equilibrium lines of different authors with varying sediment fractions between sand:silt:clay respectively.

From the last discussion, the third research question can be answered by stating that the addition of clay particles enhances even further than silt the transport efficiency of sand in density flows.

Implications for turbidite depositional architecture

The architecture of natural turbidite systems is not only controlled by the amount of sediment supply and type of continental-margin controlled (Covault et al 2012) but also by sediment input (Reading & Richards, 1994), and intrinsic sediment-gravity-flow dynamics (Covault et al, 2012).

Figures 22 and 23 show data highly comparable to the idea of having sediment input as an important controller of natural depositional architectures. Sandy systems, on one hand, are characterized by having short run-out distances and being associated with higher slope angles, (Reading and Richards, 1994). These experiments have demonstrated that pure sandy currents reach the equilibrium stage at higher slopes causing the system to be shorter. On the other hand, mixed experimental flows, have much lower equilibrium slopes. This is an effect of the clay that causes that the viscosity increases allowing the flow to maintain sand in suspension and develop extended systems.

Following Covault`s et al. 2012 the relationship between continental-margin relief (measured from proximal canyon heads to distal channel termini) and canyon-and-channel length (Equations 1 and 2) is no-linear. The authors suggest that this non-linearity can be related with internal flow dynamics such as velocity and concentration. This work has shown that the addition of clay causes the flow to get lower velocities compared to pure sandy flows and to lower the equilibrium slope. This observations not only suggest that clay affects the length of the system, but also the velocity at which the flow moves, thus, slow muddy flows produce longer systems whereas rapid flows are associated with short run-outs. The reason why the velocity will also affect the length of the system remains unknown but this work confirms the ability of clay to modify fluid-internal properties and explain the non-linearity that Covault et al (2012) have suggested.

Facies distribution

In this section each experiments is considered to be a window along the continental slope to the basin plane in real-world systems (Figure 24A). This means that the experiments performed at higher slopes angles represent areas closer to the continental shelf whereas experiments that run at lower slope angles are interpreted to be closer to the abyssal plain. In this way a facies tract chart (Figure 24B) was constructed using the pattern in thickness, sedimentation rates and sediment fraction of both sets 2 and 3 (Figure 16 to 20).

Is important to mention that in nature subaqueous flows can transform their fluid-properties as they incorporate by erosion sufficient mud that influences their fluid-dynamics (Haughton et al, 2009) and also their depositional behavior. The last is represented in the facies tract by blue arrows that indicate that the character of the deposits along the continental slope to the basin plain can change depending on how much mud is incorporated at certain moment.

Thickness and sedimentation rates analysis

Sandy currents generate both tail and body sand deposits at high sedimentation rates in proximal areas , whereas clay-laden currents with at least 30% clay volume concentration generate tail deposits with low sedimentation rates in the same area. Still, clay laden flows will generate thick body-deposits with relatively higher sedimentation rates in distal areas from the coast.

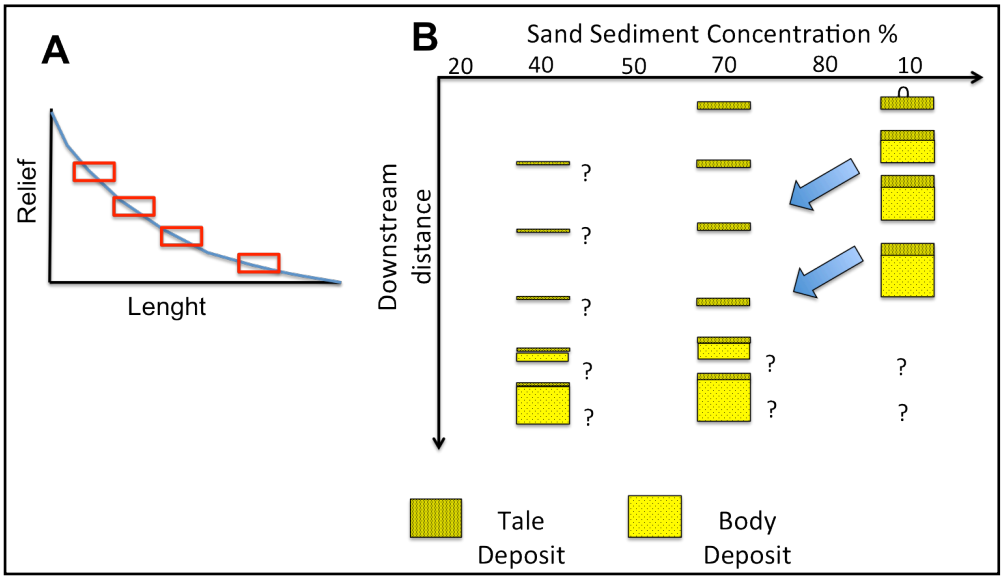

Fig. 24 A. Representation of experiments along the continental slope till the abysssal plain. B.Facies tract chart.

The thickness distribution of the body-sand packages along the continental slope to the basin plain can also be predicted by the outcome of these experiments. Here, under pure sandy flows the thickest packages occur at higher slope angles (meaning proximal areas in real nature), whereas in flows with concentrations sand70% - clay 30%, the thickest packages of sand are inferred to be deposited in distal areas.

The field work data of Wynn et al. (2002) in The Moroccan Turbidite System, (MTS), on the north-west African margin, shows sand-packages thickness distribution along the seafloor in a similar manner as here (Figure 25). The MTS is one of the largest turbidite systems in the world and has an excellent core control that enabled a detail insight in the turbidite depositional architecture, the two schematic pictures of figure 25, lie in the Agadir Basin and are linked to the Agadir Canyon. The first sketch corresponds to a turbidite of around 15km^3 in volume, which deposits are located close to the channel termination and decrease in thickness towards the basin plan. The second sketch corresponds to a larger-volume turbidite (125km^3), which maximum deposit thickness are at some distance from the canyon that feed it (Wynn et al. 2002). Although, the authors explain the two different architectures by flow volume variations, the results presented here also indicates that the addition of small amount of clay will also modify the thickness of the sandy packages along the continental slope profile. Taking into account that with higher flow-volumes the entrainment of muds by erosion of the sea-floor (Haughton et al, 2009), can increase significantly the carrying capacity of the flow, thicker sand deposits will occur further into the abysssal plain. In this way, both of the hypothesis to explain thickness variations along the continental

slope profile (flow-volume and clay content) are both consistent with the distribution of the MTS deposits.

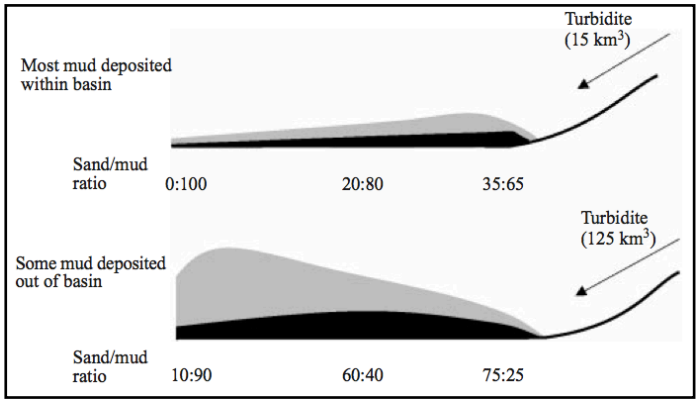

Figure 25. Schematic diagram showing the depositional architecture of two turbidites in the Agadir Basin. Black arrows indicate turbidity current flow direction. Diagram no to scale. Modified from Harris et al. (2002), after Wynn et al. (2002).

Quality of Tail and body deposits

One of the most important findings of this work is the fact that muddy flows can create clean sand-packages with clay contents lower than 2.5% (Figure 19). This results answers the fourth research question of these work, by stating that very clean sand packages can be deposited from clay-laden flows. Both parts of the flow, tail and body have the ability to create very well sorted sand packages.

Other important characteristic is that the mean grain size of the input sediment is always finer than the mean grain size of the tails and these are again finer than the P50 of body sand-packages. Deposits from the tail are found in all the runs even at 9 degrees slope angle in the 70% sand sediment concentration run. This means that the tail deposits through the whole path of the flow when having a bypassing body. Once the body reaches aggrading conditions in more distal parts, the body starts to deposit coarser grained sandstones, overlaid by the accompanying more finer grained-sandstones tail deposits at the top.

From this analysis, it can be said that turbidity flows are selective currents that leave the coarser particles to be deposited in the body of the flows in more distal parts under muddy flows.

IMPLICATIONS FOR HYDROCARBONS EXPLORATION

The data obtained here has major implications for the oil and gas industry. It has been shown experimentally that muddy flows generate larger systems and are associated with lower equilibrium slopes. Also, thickness, sedimentation rates and reservoir quality are affect by the addition of clay. In this way thick coarse grained sandy-packages are generated at relatively low slopes in the lab, or distal parts in nature under a clay laden flow.On the other hand, free-clay laden flows produce thick coarse grained sandstones at higher slopes in the experiments or proximal areas in nature.

Knowing the composition of the source sediment integrated with a general estimation of how much mud can be incorporated by erosion, explorers can predict more

precisely the distribution of sand in the system and know where the thickest packages with best reservoir properties can lie.

This last would help considerably to reduce risks related with the exploration phase, such us reservoir presence, reservoir quality and seal capacity. Also, having a general estimation of the clay component in the flow can help to create an initial filter to consider a project economically viable, since then more muddy the system is then more distal the sands are and this implies higher costs in drilling, transporting and producing the reserves.

Furthermore, these work has probed that the outcome of experimental work is highly in accordance with data from outcrops and present-day ocean floor systems architecture. Besides, doing experiments in the laboratory is in many cases safer and cheaper than performing acquisition of data in actual destructive powerful turbidity-currents. In this way, more laboratory experiments are needed in order to better understand turbidite reservoirs, and thus oil and gas industry should keep focusing on these kind of learning.

RECOMMENDATIONS FOR FURTHER RESEARCH

Even though the findings obtained from the data contained in this report are quite relevant for the understanding of deep-water deposits, there are still a lot of things that need to be done.

It is important to create a larger data base of experiments to fill with real data the assumptions made in figure 24 (represented with question marks). By doing this, important characteristics of the deposits can be studied and then applied to nature. For example, how is the pattern of the thickness of the deposits further into the abyssal plain (in the lab, slopes bellow 3), would they transitionally become thinner or would they maintain the same thickness and have a sharp ending.

Also, by testing different sand:clay proportions, for example 50%Sand 50%Clay, the carry capacity of high clay-laden flows can be tested again and in case it confirms the results presented here, it will not only give stronger evidence to probe that clay particles produce extensive systems but maybe to establish a quantitative relationship between clay concentration and location of maximum sand thickness, at least in the map. The main goal would be to scale the experimental results with nature.

Since the clay has a large effect in velocity, is important to know exactly what kind of changes it causes and at which proportions. From Baas et al (2002) and results showed here, it is know the the main changes occur in the internal part of the flow. However the outcome of these experiments have a lot of uncertainty in the data quality of the inner region, so in further experiments a UVP sensor must be located at the very base in order to capture this variations. By locating the UVP in this area, analysis on shear velocities and turbulence intensity can give new insights on the dynamics in the inner region.

These experiments used only two grain sizes (D50 = 190um and D50 =7.7um). Mixing of multiple grain sizes is also of interest. Also would be important to introduce some tracer particles to see what kind of sedimentary structures and turbulence behavior the fluid has when incorporating different grain sizes.

Conclusions

Closed-channel fluid dynamics reveal to be comparable to open-channel flow-dynamics. At a constant discharge between 58m^3/h and 72m^3/h, the experimental flows pass through the four of the five phases described by Baas et al (2009) as clay concentration increases: (1) turbulent flow; (2) turbulence-enhanced transitional flow; (3) lower transitional plug flow (non-observed); (4) upper transitional plug flow; and (5) quasi-laminar plug flow. The transition from phase to phase depends on the concentration of clay, since clay has the capacity of suppressing local shear stresses, and thus reduce velocity gradient and turbulence intensity.

Transition between aggrading to non-aggrading current behavior is a function of sediment fraction. The increment in clay content causes the equilibrium slope to decrease even lower than with the addition of silt, indicating the ability of kaolinite to maintain sediments in suspension and restrict the deposition of sand even at very low slopes.

When looking at the experiments as a window along the continental slope to the basin plane in real-world systems, the results reveal that thick coarse grained sandy-packages are generated at relatively low slopes in the lab, or distal parts in nature under a clay laden flow. On the other hand, free-clay laden flows produce thick coarse grained sandstones at higher angle slopes in the laboratory or proximal areas in nature.

Clean sand packages can be deposited from clay-laden flows. Both parts of the flow, tail and body have the ability to create very well sorted sand packages.

Acknowledgments

This thesis was accomplished as part of my degree as Master of Science in Geology at the Faculty of Earth Sciences at the Utrecht University. For the success of this project, I would like to thank:

Dr. J. T. Eggenhuisen, for his supervision, opportunity to perform my experiments in the Eurotank, many fruitful discussions, feedback, enthusiasm and contagious passion for deep water avalanches.

Dr. Matthieu Cartigny, for his help to improve the manuscript with productive comments and valuable criticism and for his help during the early phase of the experiments.

Thony van der Gon Netscher, for supplying all materials and equipment and his efficient way of solving experimental problems in a very short time.

Henk van der Meer, for his great support on solving numerous ICT-problems

Natan Cheshier, Frediano Clos, Matia Gilio, Jan de Leeuw, Jochem Bijkerk, and Alex Prent for all their help during the experimental phase, without them, the acquisition data would have been a horrible failure.

Besides the scientific part of the Masters, my stay in Utrecht resulted in a lot of personal friendships and experiences with people from different nationalities. You all made my perspective of the world broader and somehow have influenced my way to enjoy and take the best of every experience including my thesis.

References

Albertão, G.A., Mulderb, T and Rémi Eschardc. (2011) Impact of salt-related palaeotopography on the distribution of turbidite reservoirs: Evidence from well-seismic analyses and structural restorations in the Brazilian offshore. Marine and Petroleum Geology, 28, 1023-1046.

Altinakar, M.S., Graf, W.H. and Hopfinger, E.J. (1996) Flow structure in turbidity currents. Journal of Hydraulic Research, 34, 713.

Baldock, T.E., Tomkins, M.R., Nielsen, P. and Hughes, M.G. (2004) Settling velocity of sediments at high concentrations. Coastal Engineering, 51, 91-100.

Baas, J.H., and Best, J.L. (2002) Turbulence modulation in clay-rich sediment-laden flows and some implications for sediment deposition. Journal of Sedimentary Research, 72, 336–340.

Baas, J.H., and Best, J.L. (2008) The dynamics of turbulent, transitional and laminar clay-laden flow over a fixed current ripple. Sedimentology, 55, 635–666.

Baas, J.H., Best, J.L., Peakall, J. and Wang, M. (2009) A phase diagram for turbulent, transitional, and laminar clay suspension flows. Journal of Sedimentary Research, 79, 162-183.

Baas, J.H., Best, J.L. and Peakall, J. (2011) Depositional processes, bedform development and hybrid bed formation in rapidly decelerated cohesive (mud--sand) sediment flows. Sedimentology, 58, 1953-1987.

Best, J.L (1992) Sedimentology and event timing of a catastrophic volcaniclastic mass flow, Volcan Hudson, Southern Chile. Bulletin of Volcanology, 54, 299-318.

Best, J.L., Kirkbride, A.D. and Peakall, J. (2001) Mean flow and turbulence structure of sediment-laden currents: new insights using ultrasonic Doppler velocity profiling. In: Particulate Gravity Currents (Eds. W.D. McCaffrey, B.C. Kneller and J. Peakall), Int. Assoc. Sedimentol. Spec. Publ., 31, 159–172.

Cartigny, M. (2012) Morphodynamics of supercritical high-density turbidity currents. PHD dissertation, University Utrecht.

Choux, C.M.A., Baas, J.H., McCaffrey, W.D. and Haughton, P.D.W. (2005) Comparison of spatio–temporal evolution of experimental particulate gravity flows at two different initial concentrations, based on velocity, grain size and density data. Sedimentary Geology, 179, 49-69.

Coussot, P. (1995) Structural similarity and transition from Newtonian to non-Newtonian behavior for clay-water mixtures. Physical Review Letter, 74, 3971–3975.

Covault, J.A., Shelef, E., Traer, M., Hubbard, S.M., Romans, B.W., and Fildani, A. (2012) Deep-water channel run-out length; insights from seafloor geomorphology: Journal of Sedimentary Research, 82, 25-40.

Eggenhuisen, J.T. and McCaffrey, W.D. (2012) The vertical turbulence structure of experimental turbidity currents encountering basal obstructions: implications for

vertical suspended sediment distribution in non-equilibrium currents. Sedimentology 59, 1101-1120.

Eggenhuisen, J. T., & McCaffrey, W. D. (2009). The depositional signature of moving hydraulic jumps in supercritical turbidity currents: Experimental suggestions for the origin of vertical transitions in turbidite. 33rd International Association of Hydraulic Engineering & Research (IAHR) Congress: Water Engineering for a Sustainable Environment.

Ferguson, R.I. and Church, M. (2004) A Simple Universal Equation for Grain Settling Velocity. Journal of Sedimentary Research, 74, 933-937.

Gladstone, Phillips and Sparks. (1998) Experiments on bidisperse, constant-volume gravity currents: propagation and sediment deposition. Sedimentology, 45, 833-843.

Harris, T.C., Hogg, A.J. and Huppert, H.E. (2002) Polydisperse particle-driven gravity currents. Journal of Fluid Mechanics, 472, 333-371.

Haughton, P., Davis, C., McCaffrey, W. and Barker, S. (2009) Hybrid sediment gravity flow deposits – Classification, origin and significance. Marine and Petroleum Geology, 26, 1900-1918.

Hodson, J.M. and Alexander, J. (2010) The Effects of Grain-Density Variation on Turbidity Currents and Some Implications for the Deposition of Carbonate Turbidites. Journal of Sedimentary Research, 80, 515- 528.

Hofstra, M. (2011) On Bidisperse Grain Size Distributions in High Density Turbidity Currents, MSc-thesis, University Utrecht.

Kneller, B. (2003) The influence of flow parameters on turbidite slope channel architecture. Marine and Petroleum Geology, 20, 901-910.

Kneller, B. and Buckee, C. (2000) The structure and fluid mechanics of turbidity currents: a review of some recent studies and their geological implications. Sedimentology, 47(Suppl.), 62–94.

Kneller, B.C., Bennett, S.J. and McCaffrey, W.D. (1999) Velocity structure, turbulence and fluid stresses in experimental gravity currents. J.Geophys.Res., 104, 5381-5391.

Lowe, D.R. and Guy, M. (2000) Slurry-flow deposits in the Britannia Formation (Lower Cretaceous), North Sea: a new perspective on the turbidity current and debris flow problem. Sedimentology, 47, 31–70.

Leeder, M. (1999) Sedimentology and Sedimentary Basins; From Turbulence to Tectonics: Oxford, U.K., Blackwell Science, 608 p.

Maciel, G. de F., Santos, Kiryu dos Santos, H. and Ferreira, F.O. (2009). Rheological analysis of water clay compositions in order to investigate mudflows developing in canals. Journal of the Brazilian Society of Mechanical Sciences and Engineering, 31, 64-74.

McCaffrey, W.D., Choux, C.M., Baas, J.H. and Haughton, P.D.W. (2003) Spatio-temporal evolution of velocity structure, concentration and grain-size stratification

within experimental particulate gravity currents. Marine and Petroleum Geology, 20, 6-8, 851-860.

McHargue, T., Pyrcz, M.J., Sullivan, M.D., Clark, J.D., Fildani, A., Romans, B.W., Covault, J.A., Levy, M., Posamentier, H.W. and Drinkwater, N.J. (2011) Architecture of turbidite channel systems on the continental slope: Patterns and predictions. Marine and Petroleum Geology, 28, 3, 728-743.

Meiburg, E. and Kneller, B. (2010) Turbidity Currents and Their Deposits. Annual Review of Fluid Mechanics, 42, 135-156.

Middleton, G.V. (1993) Sediment deposition from turbidity currents. Annual Review of Earth & Planetary Sciences, 21, 89-114

Middleton, G.V., (1967) Experiments on density and turbidity currents. III. Deposition of sediment, Canadian Journal of Earth Sciences, 4, 475-505

Middleton, G.V., (1966) Experiments on Density and Turbidity Currents: I. Motion of the Head, Canadian Journal of Earth Sciences, 3:(4), 523-546

Mueller, S., Llewellin, E.W. and Mader, H.M. (2010) The rheology of suspensions of solid particles. Proceedings of the Royal Society A: Mathematical, Physical and Engineering Science, 466, 1201-1228.

Mulder, T. and Alexander, J. (2001) The physical character of subaqueous sedimentary density flows and their deposits. Sedimentology, 48, 269-299.

Nezu, I. and Nakagawa, H. (1993) Turbulence in Open-Channel Flows: Delft Hydraulics, International Association for Hydraulic Research, Monograph, p 58-59.

Nourmohammadi, Z., Afshin, H. and Firoozabadi, B. (2011) Experimental observation of the flow structure of turbidity currents. Journal of Hydraulic Research, 49, 168-177.

Peakall J, Asworth P and Best J (1996) Physical Modelling in Fluvial Geomorphology: Principles, Applications and Unresolved Issues.

Postma, G. (1986) Classification for sediment gravity-flow deposits based on flow conditions during sedimentation. Geology, 14, 291-294.

Reading, H.G and Richards, M. (1994) Turbidite systems in deep-water basin margins classified by grain size and feeder system. American Association of Petroleum Geologists, Bulletin, 78, 792–822

Salaheldin, T.M., Imran, J., Chaudhry, M.H. and Reed, C (2000) Role of fine-grained sediment in turbidity current flow dynamics and resulting deposits, Marine Geology, 171/1-4, 21-38

Sequeiros, O.E., Spinewine, B., Beaubouef, R.T., Sun, T., Garcia, M.H. and Parker, G. (2010) Bedload transport and bed resistance associated with density and turbidity currents. Sedimentology, 57, 1463- 1490.

Shin, J.O., Dalziel, S.B. and Linden, P.F. (2004) Gravity currents produced by lock exchange. Journal of Fluid Mechanics, 521, 1-34.

Stacey, M.W. and Bowen, A.J. (1988) The Vertical Structure of Density and Turbidity Currents: Theory and Observations. J.Geophys.Res., 93, 3528-3542.

Sumner, E.J., Amy, L.A. and Talling, P.J. (2008) Deposit Structure and Processes of Sand Deposition from Decelerating Sediment Suspensions. Journal of Sedimentary Research, 78, 529-547.

Wan, Z.H and Wang, Z.Y (1994). Hyperconcentrated Flow: Rotterdam, A.A. Balkema, 320.

Wang, Z and Plate, E.J (1996). A preliminary study on the turbulence structure of flows on non-Newtonian fluid: Journal of Hydraulic Research, v. 34, p. 345–361.

Wang, Z.H. and Larsen, P. (1994) Turbulence structure of flows of water and clay suspensions with bedload. Journal of Hydraulic Engineering. 120, 577-600.

Wetzel, A. (1993) The transfer of river load to deep-sea fans: a quantitative approach. American Association of Petroleum Geologists, Bulletin. 77, 1679–1692.

Wynn, R. B., Weaver, P. P. E., Masson, D. G. & Stow, D. A. V. (2002) Turbidite depositional architecture across three interconnected deep-water basins on Northwest African margin. Sedimentology. 49, 661–695.

Xu, J.P. (2010) Normalized velocity profiles of field-measured turbidity currents. Geology. 38, 563-566-